Elena (1985)

WMO Training Course on Tropical Cyclones

La Réunion (September 2017)

1. **Internal structure**
2. **External influences**
3. **Inter-annual & intra-seasonal variability**
4. **Climatic changes**

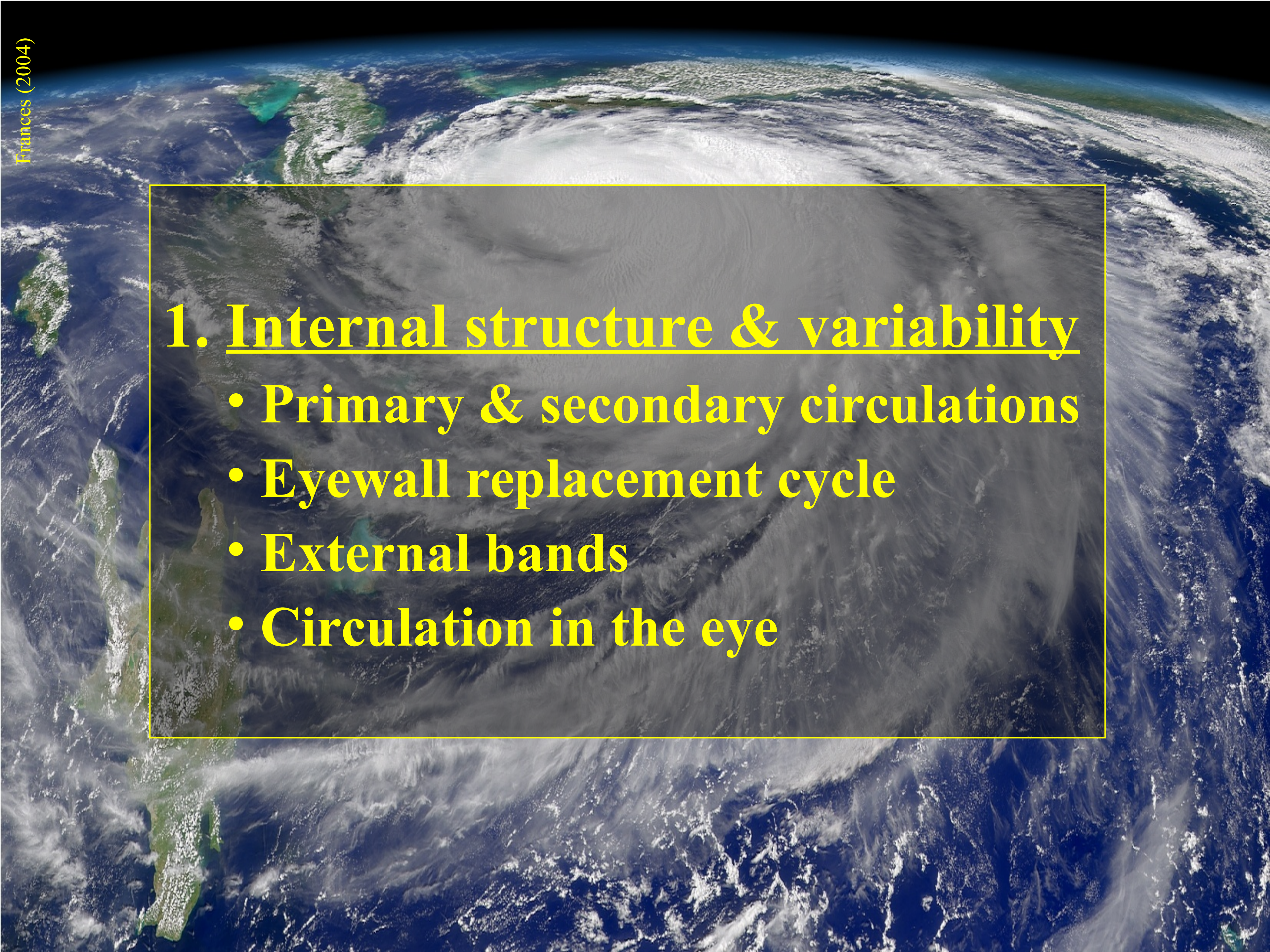

Frances (2004)

1. <u>Internal structure & variability</u>

- **Primary & secondary circulations**
- **Eyewall replacement cycle**
- **External bands**
- **Circulation in the eye**

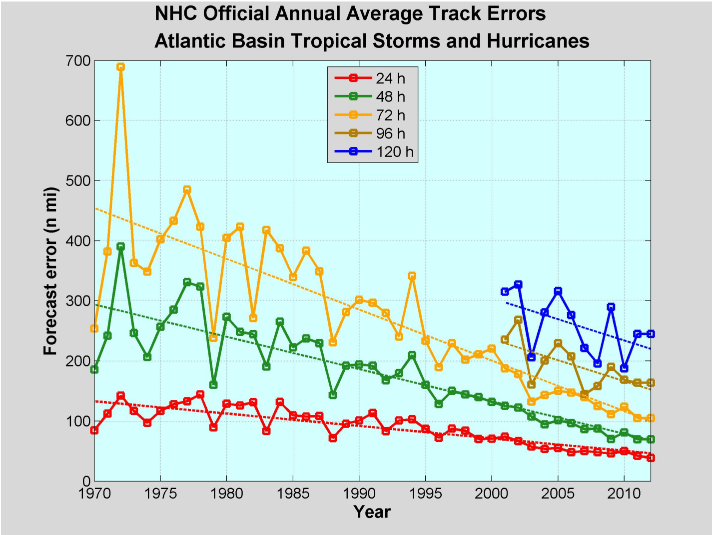

TRACK ERROR

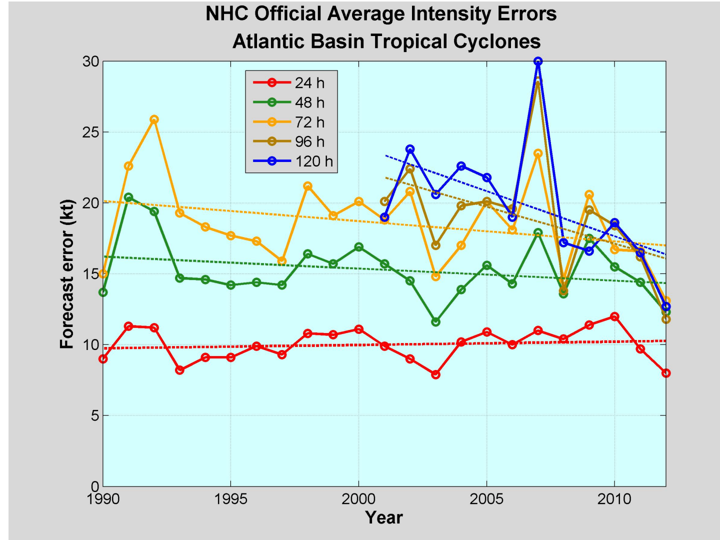

INTENSITY ERROR

Evolution of average mean absolute errors for official TC track and intensity predictions at various lead times in the North Atlantic basin

Which factors control the intensity of tropical cyclones ?

- <u>Internal</u> : thermodynamics and dynamics of the eyewall and of the external rainbands, …

- <u>External</u> : SST, wind shear, dry zones, upper-level features, + landfall, extra-tropical transition, …

INSIDE TROPICAL CYCLONES

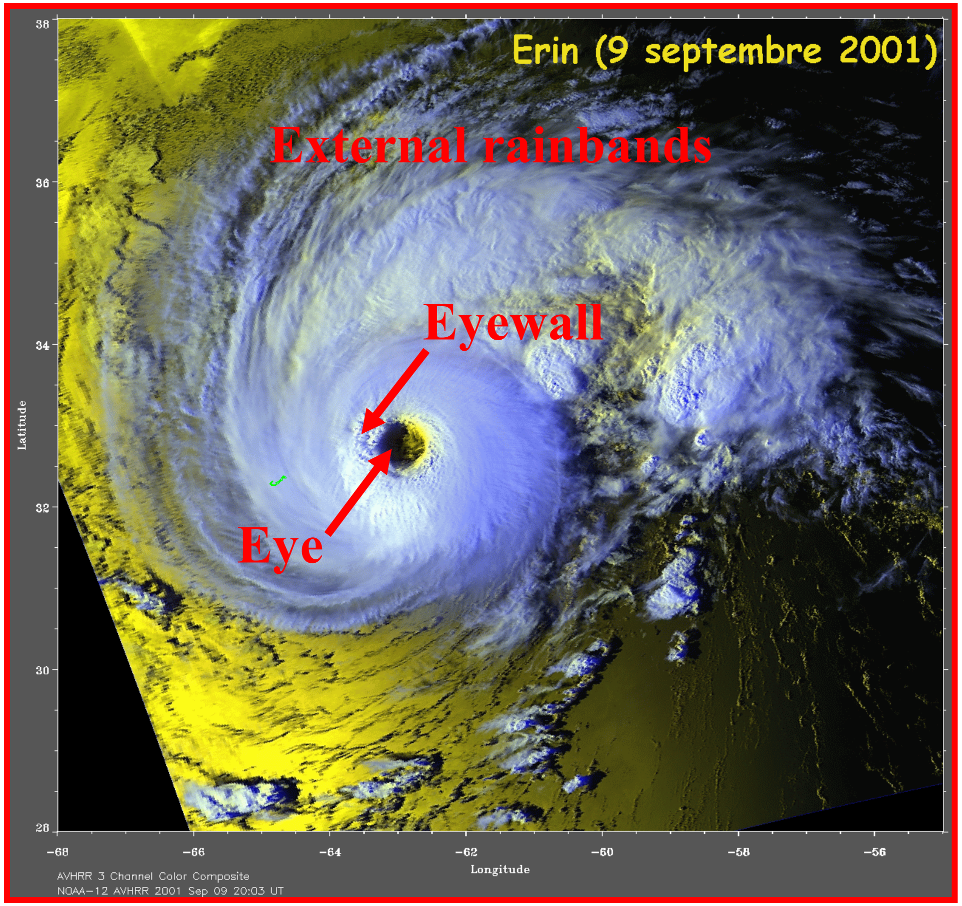

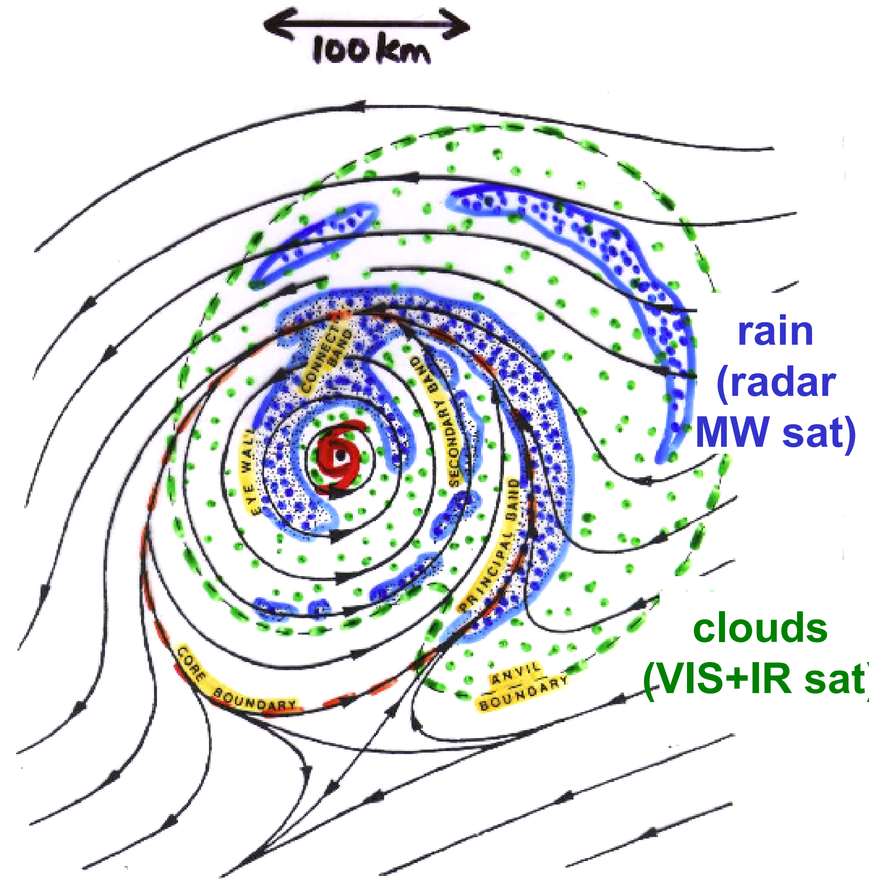

<u>Primary circulation</u> : tangential (few 10 m/s)

<u>Secondary circulation</u> : radial and vertical (few m/s)

THE PRIMARY CIRCULATION

The centrifugal acceleration of the wind ( ) balances the centripetal force toward the central pressure low **(D)** ;

The central pressure low **(D)** results from the presence of warm air aloft in the eye ;

→THERMAL WIND BALANCE : $\partial V_T/\partial z \propto \partial \theta/\partial r$

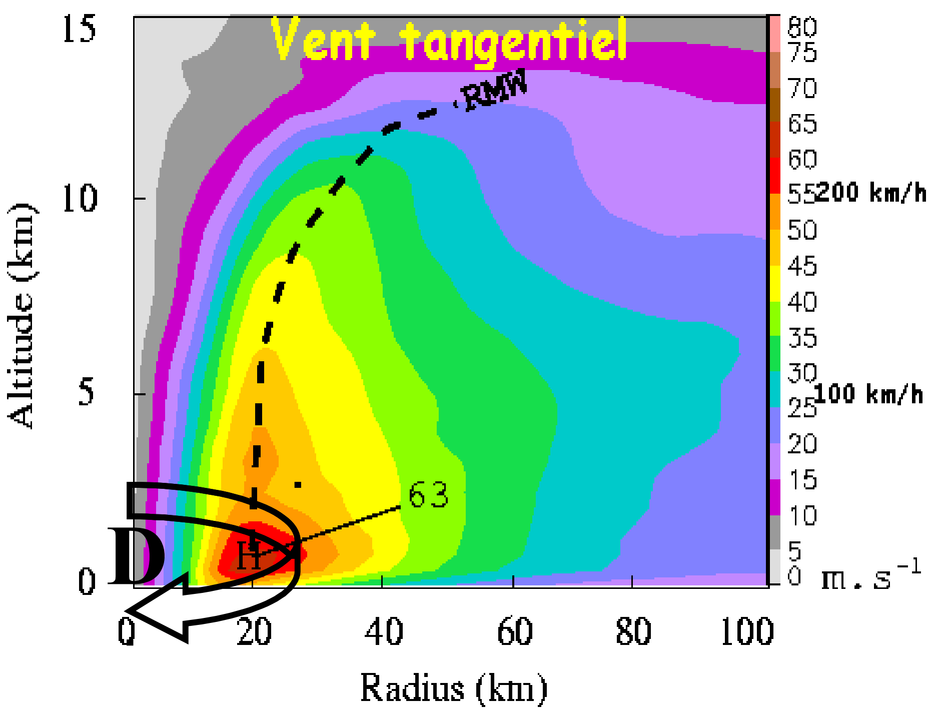

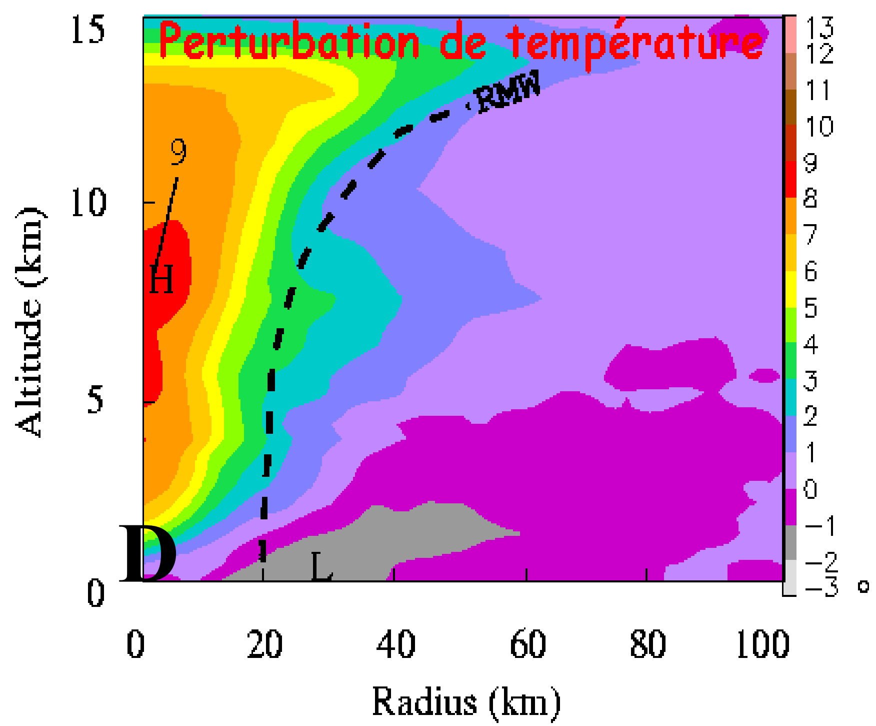

TROPICAL CYCLONE AS A HEAT ENGINE :

The equivalent « Carnot Cycle » [Emanuel, 1986 : *J. Atmos. Sci.*, 43, 585-604]

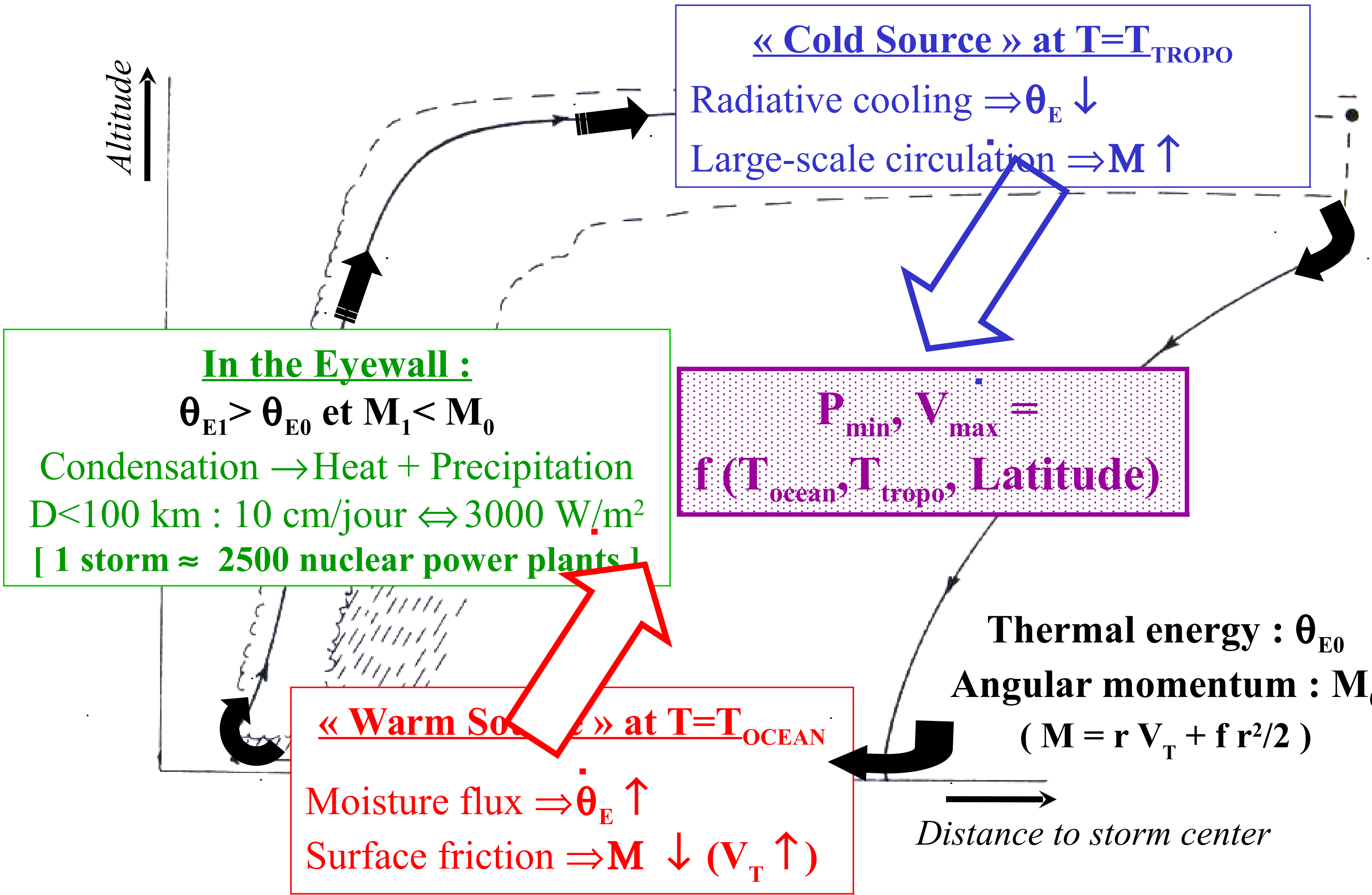

TROPICAL CYCLONE AS A HEAT ENGINE :
Climatological Maximum Potential Intensity (1)

$$P_{min} \text{ or } V_{max} = f\,(\,SST\,,\,T_{tropopause}\,,\,\text{Latitude})$$

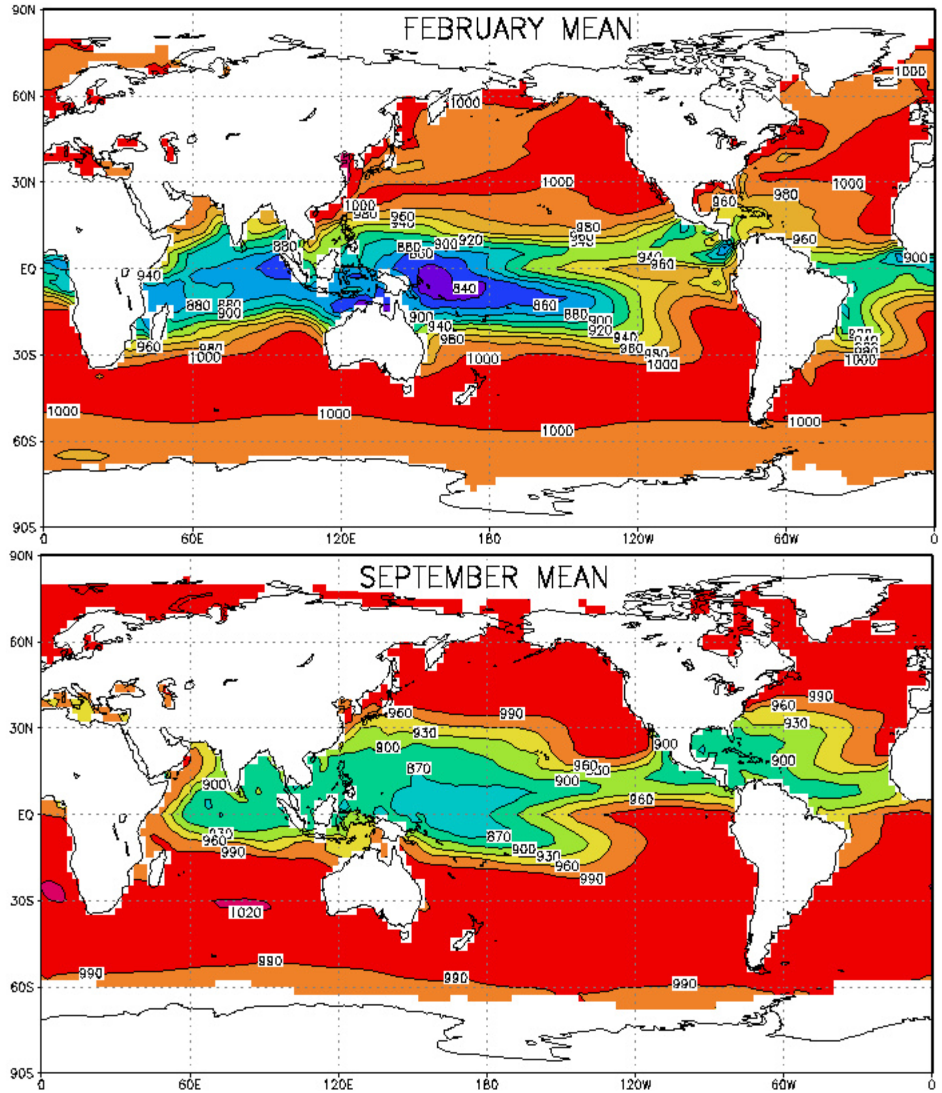

TROPICAL CYCLONE AS A HEAT ENGINE :
Air-sea interactions (1)

Heat and moisture fluxes at the ocean surface are the main sources of energy for cyclonic circulation.

The « **bulk** » **formulation** expresses these fluxes as functions of the mean flow and of **transfer coefficients** :

Sensible heat flux : $Q_S = \rho\, C_S\, |\underline{V}_{air}|\, C_P\, (T_{surf} - T_{air})$

Latent heat flux : $Q_L = \rho\, C_L\, |\underline{V}_{air}|\, L\, (q_{surf} - q_{air})$

→ ***Enthalpy flux :*** $Q_E = \rho\, C_S\, |\underline{V}_{air}|\, (H_{surf} - H_{air})$ with $H = C_P\, T + L\, q$

C_E ***= enthalpy exchange coefficient***

Momentum flux (i) : $Q_{Vi} = \rho\, C_D\, |\underline{V}_{air}|\, (V_{i\_air})$

C_D ***= surface drag coefficient***

(**ρ** = air density, $|\underline{V}_{air}|$ = wind module, **θ** = potential temperature, **q** = mixing ratio, C_P = specific heat at constant P , **L** = latent heat of vaporization)

Reciprocally, friction of the wind at surface transfers energy to the ocean through the *generation of waves et currents* at various depths.

TROPICAL CYCLONE AS A HEAT ENGINE :
Air-sea interactions (2)

Black *et al.* 2007: *Bull. Amer. Meteor. Soc.*, 88, 357-374

The enthalpy exchange coefficient $\mathbf{C_E}$ is roughly constant for winds ≤30 m/s. *It could increase beyond 40 m/s, in relation with sea spray ?*

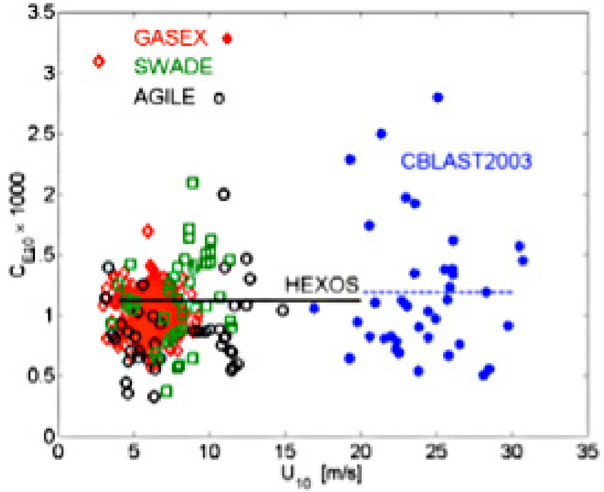

[Powell *et al.* 2003 : *Nature*, 422, 279-283]

The surface drag coefficient $\mathbf{C_D}$ reaches a maximum for a 40 m/s wind, and *slowly decreases beyond ?*

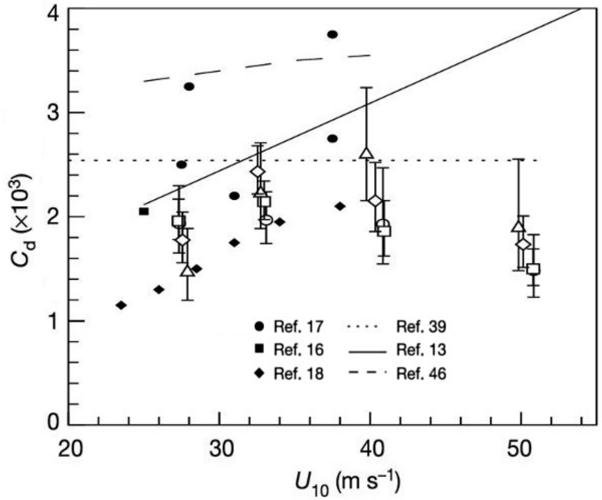

TROPICAL CYCLONE AS A HEAT ENGINE :
Air-sea interactions (3)

Chen *et al.* 2007 : *Bull. Amer. Meteor. Soc.*, 88, 311-317

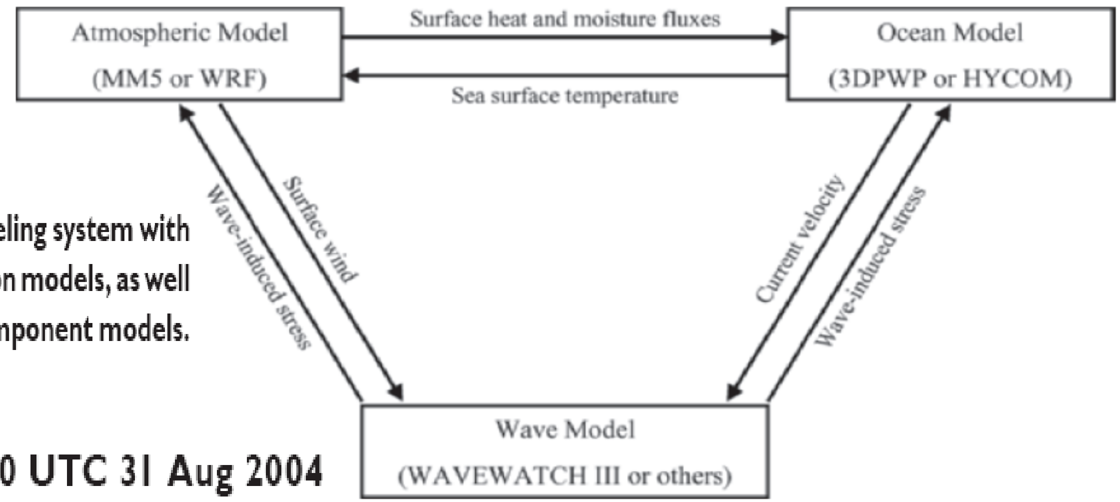

FIG. 1. Schematics of a coupled atmosphere-wave-ocean modeling system with the component atmosphere, surface wave, and ocean circulation models, as well as the coupling parameter exchanges between each of the component models.

Hurricane Frances at 1200 UTC 31 Aug 2004

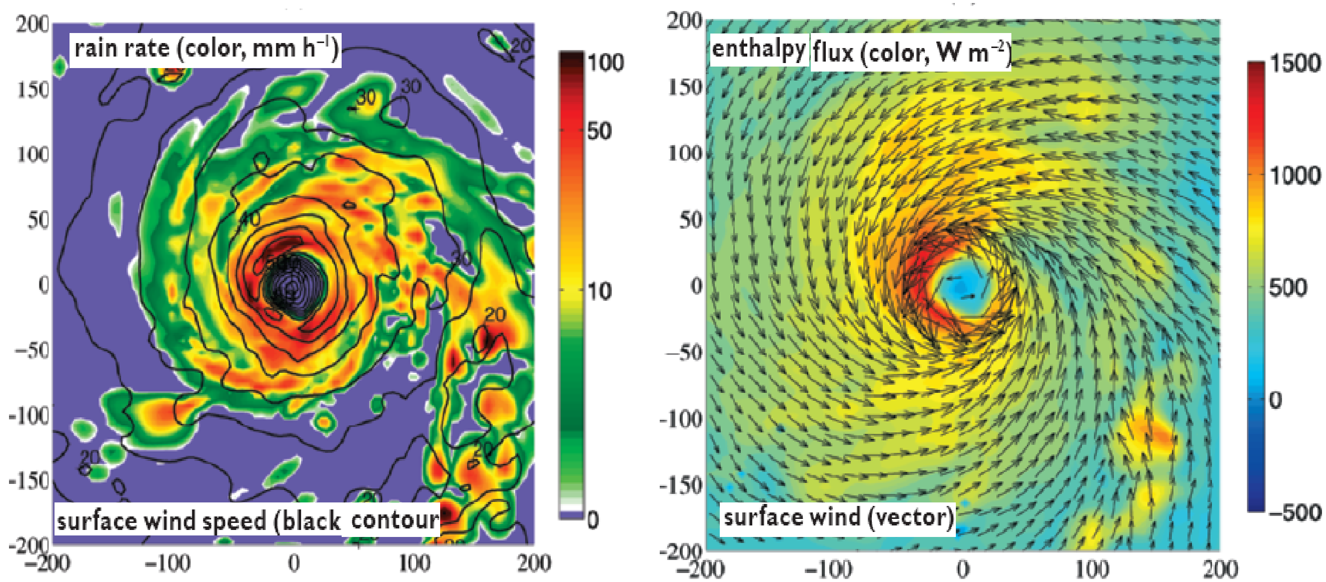

TROPICAL CYCLONE AS A HEAT ENGINE :

Air-sea interactions (4)

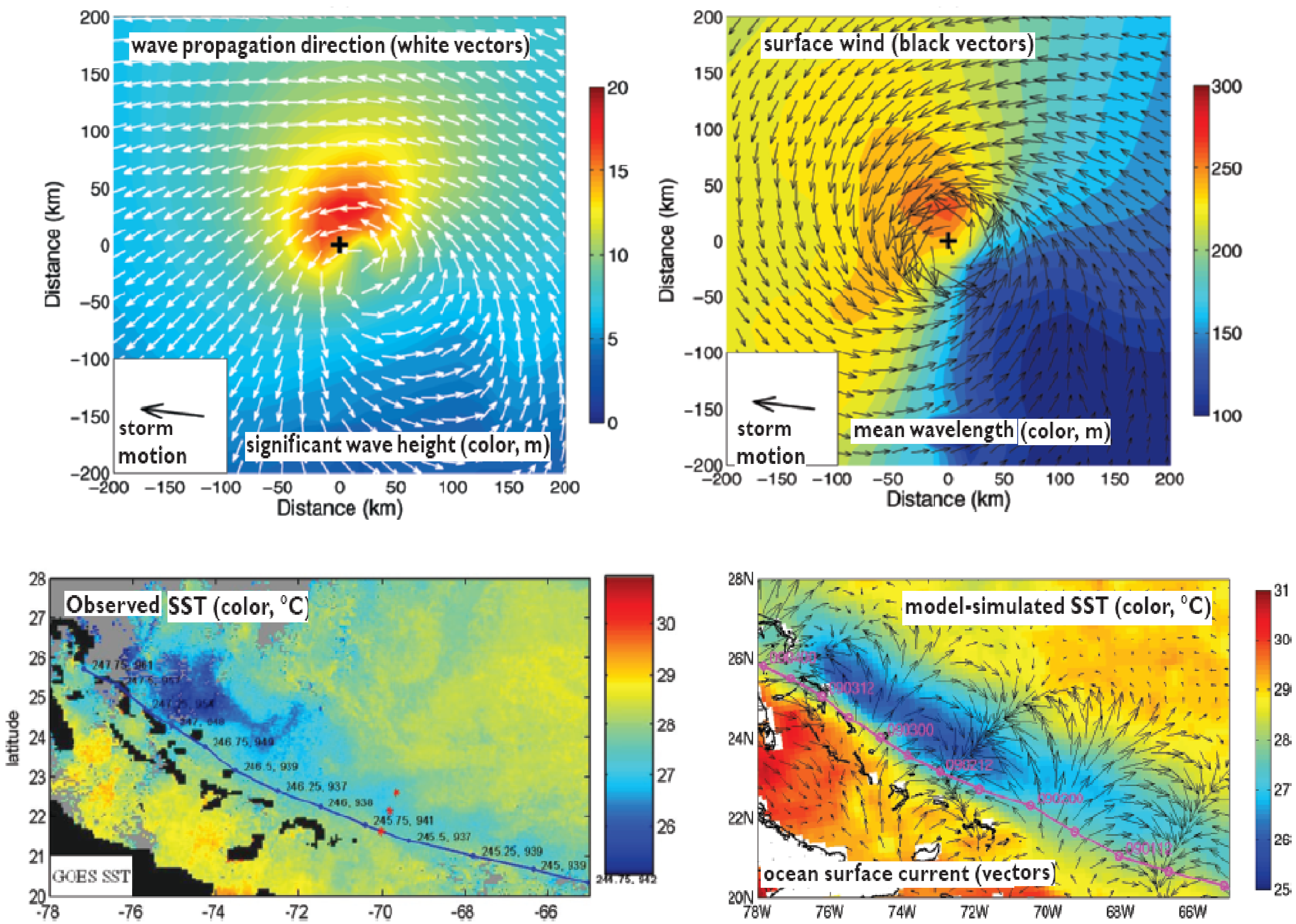

TROPICAL CYCLONE AS A HEAT ENGINE :
Pumping the upper-ocean heat (1)

Rita weakened before it reached the Texas coast

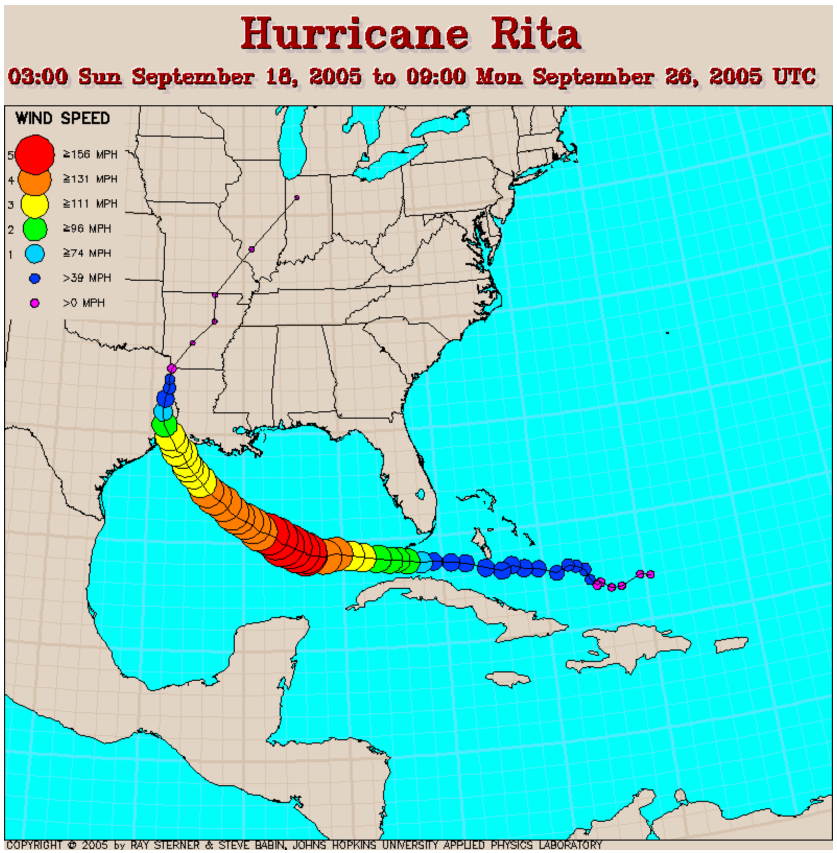

Decreasing « ocean heat content » in the Gulf of Mexico

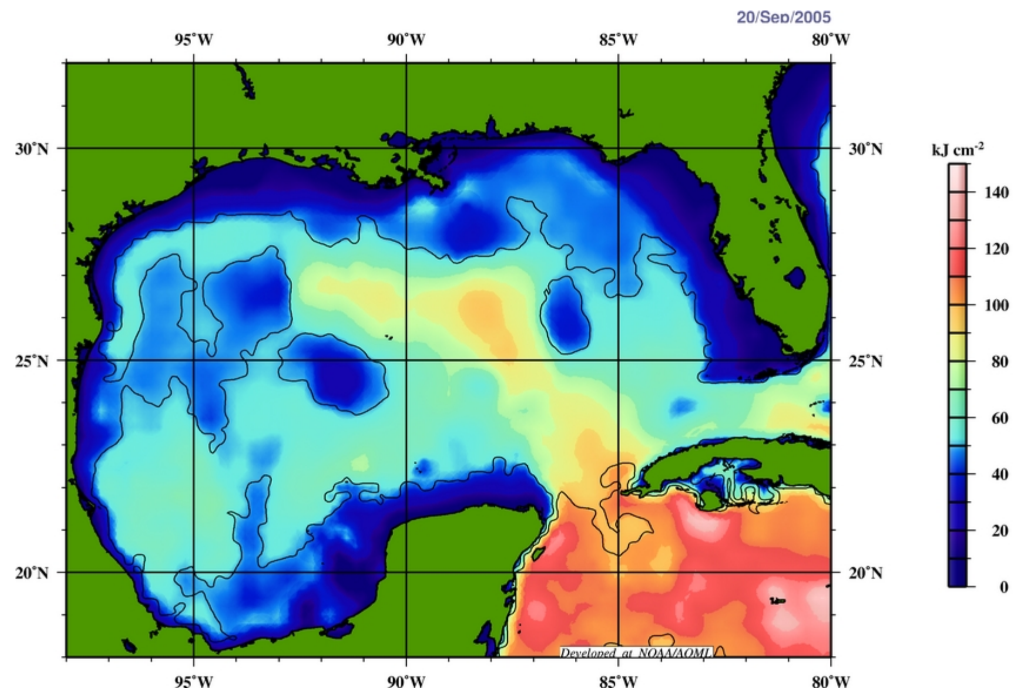

TROPICAL CYCLONE AS A HEAT ENGINE :
Pumping the upper-ocean heat (2)

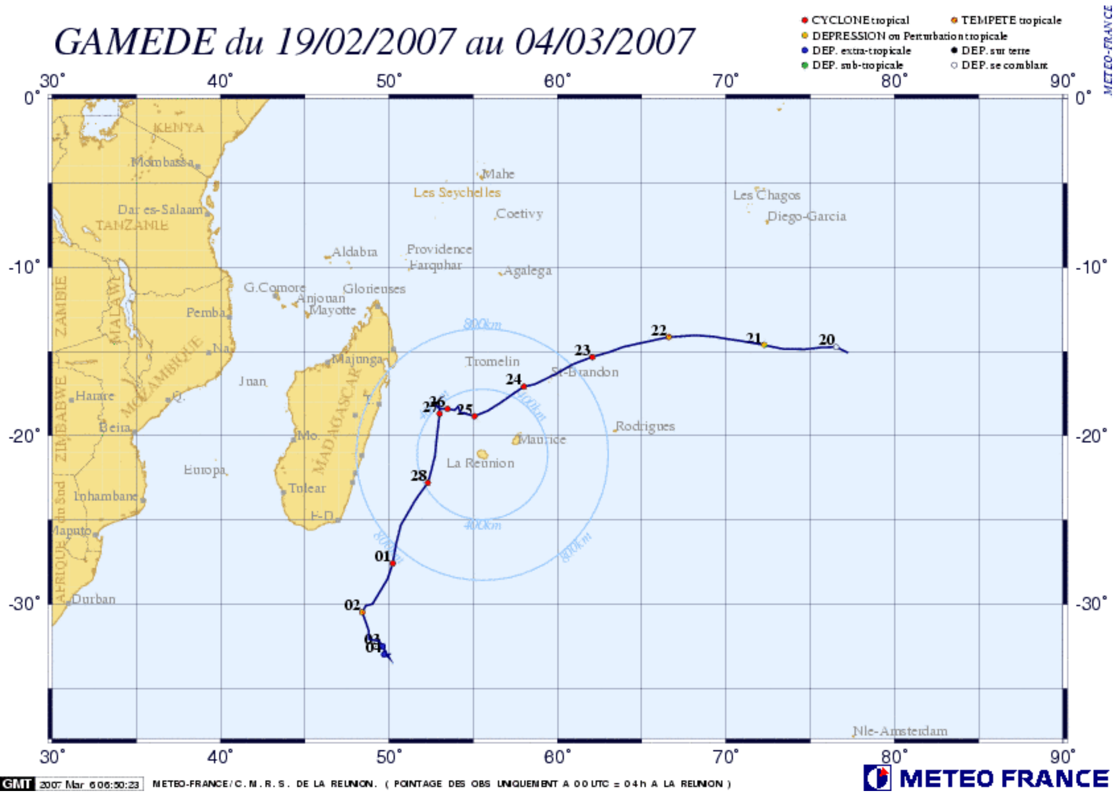

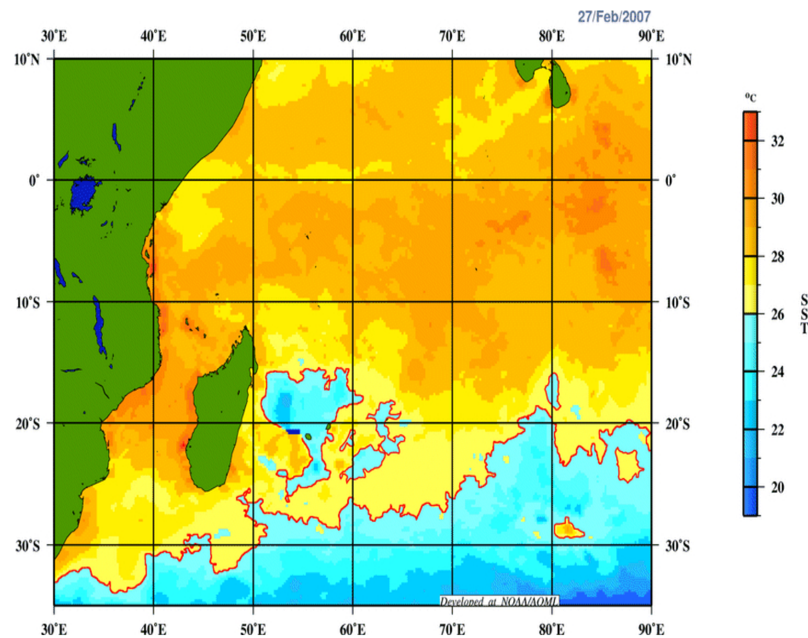

THE SECONDARY CIRCULATION

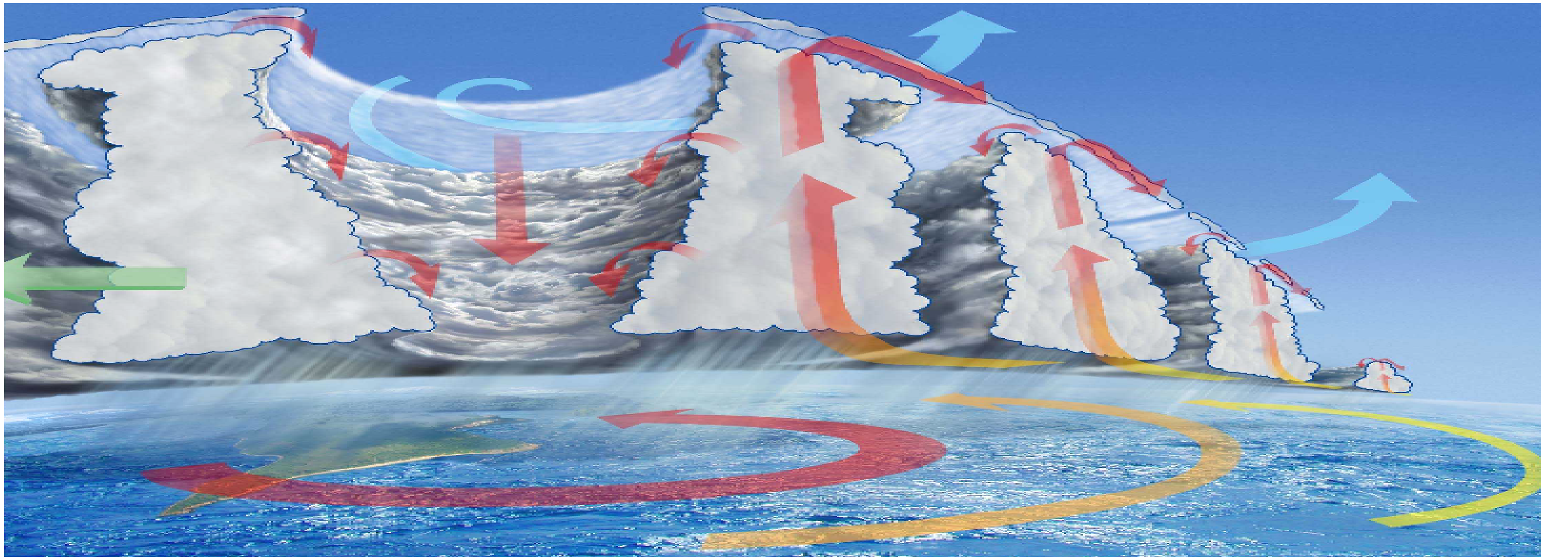

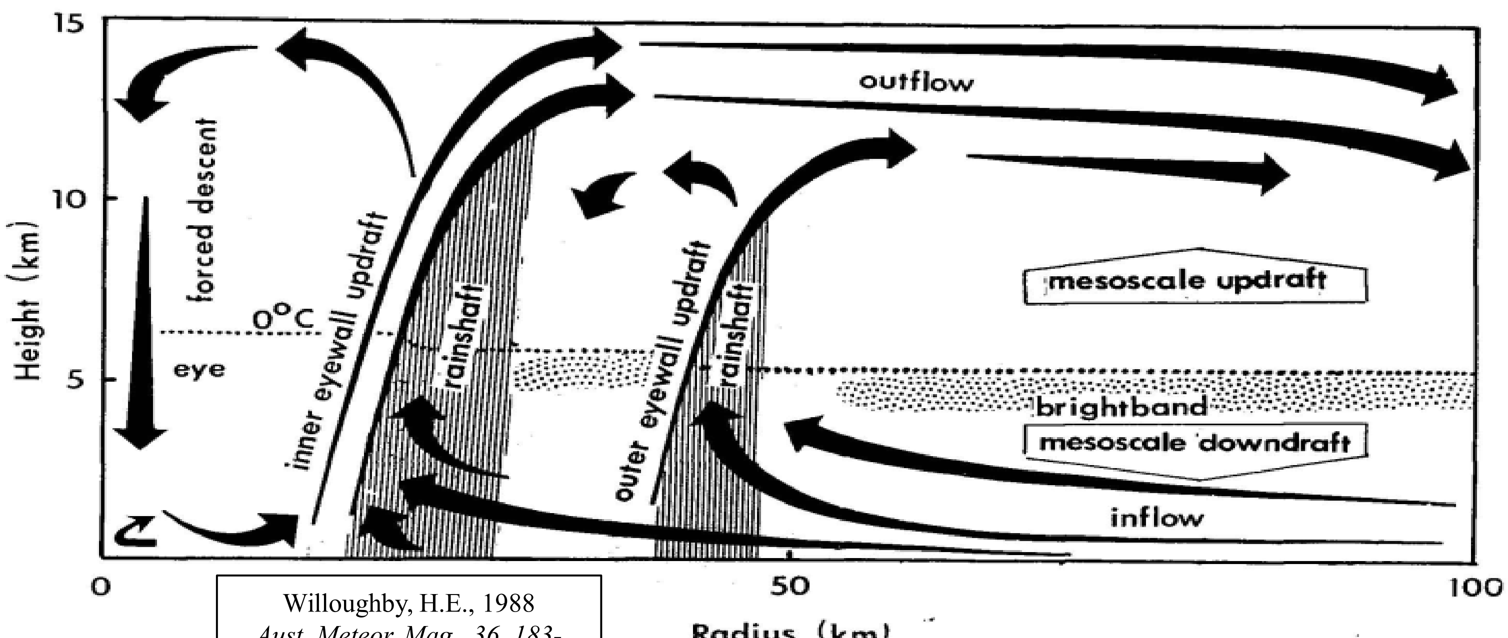

Willoughby, H.E., 1988
Aust. Meteor. Mag., 36, 183-191

THE SECONDARY CIRCULATION
Observations (1)

Jorgensen 1984 [*J. Atmos. Sci.*, 41, 1287-1311] :
a conceptual model for the inner core of Hurricane Allen (1980)

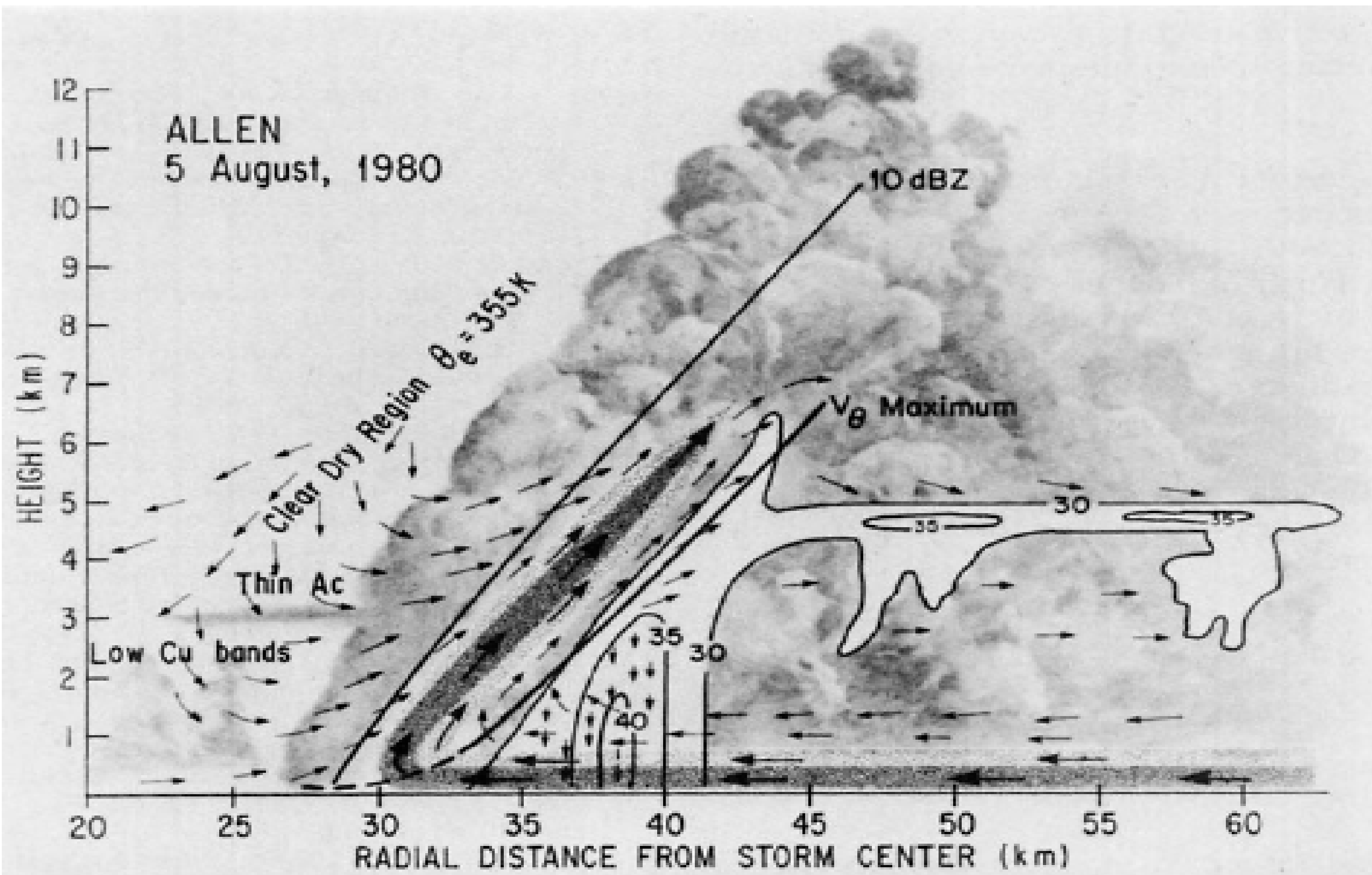

THE SECONDARY CIRCULATION
Numerical Models (1)

Liu *et al.* 1999 [*Mon. Wea. Rev.*, 127, 2597-2616]

Axisymmetric structure of Hurricane Andrew (1992) with a 6-km horizontal grid :

- moist inflow in the boundary layer, outflow in the upper troposphere,
  slantwise ascent in the eyewall where the tangential wind is maximum ;
- penetrative dry downdraft at the inner edge of the eyewall ;
- weak subsiding motion in the eye with warming/drying above an inversion ;
- below, warm/moist air coming from the low-level inflow and downdraft.

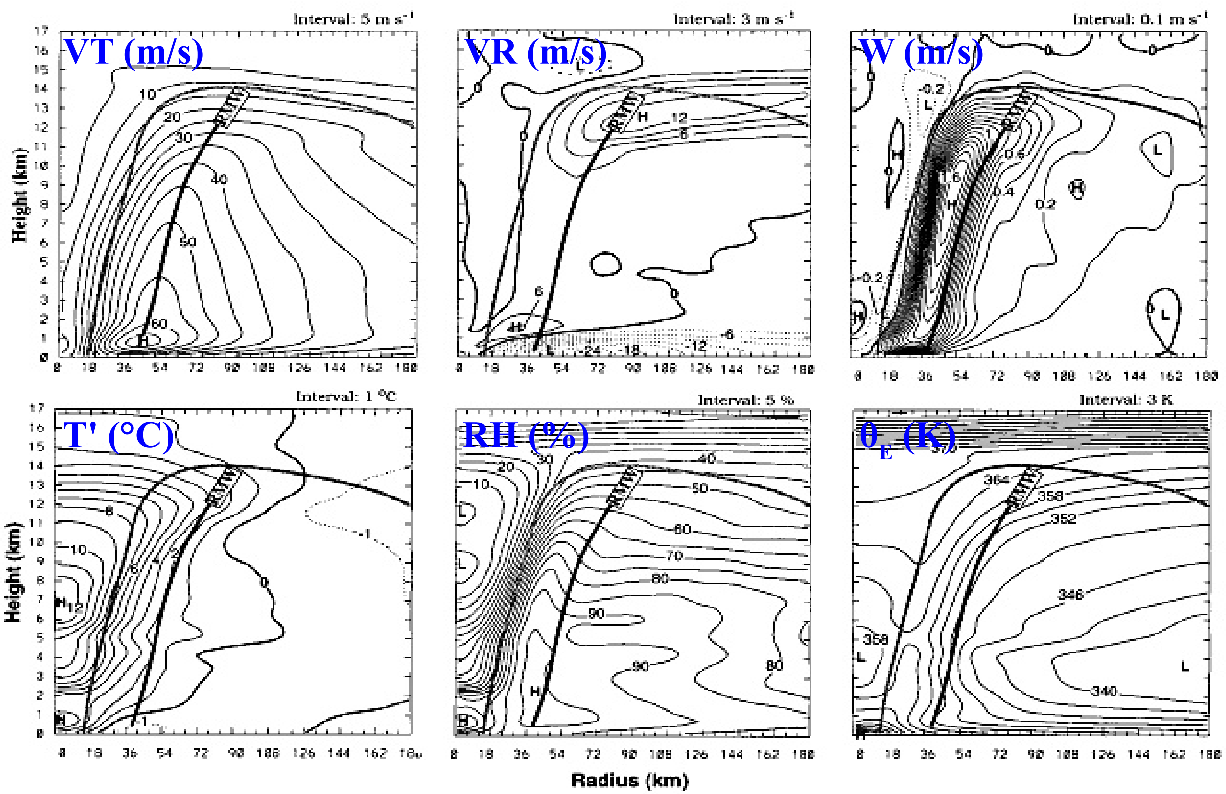

THE SECONDARY CIRCULATION
Numerical Models (2)

Yau *et al*, 2004 :
Mon. Wea. Rev., <u>132</u>, 3299-3314

Surface wind | **Surface reflectivity** | **W-E reflectivity**

6-km grid

2-km grid

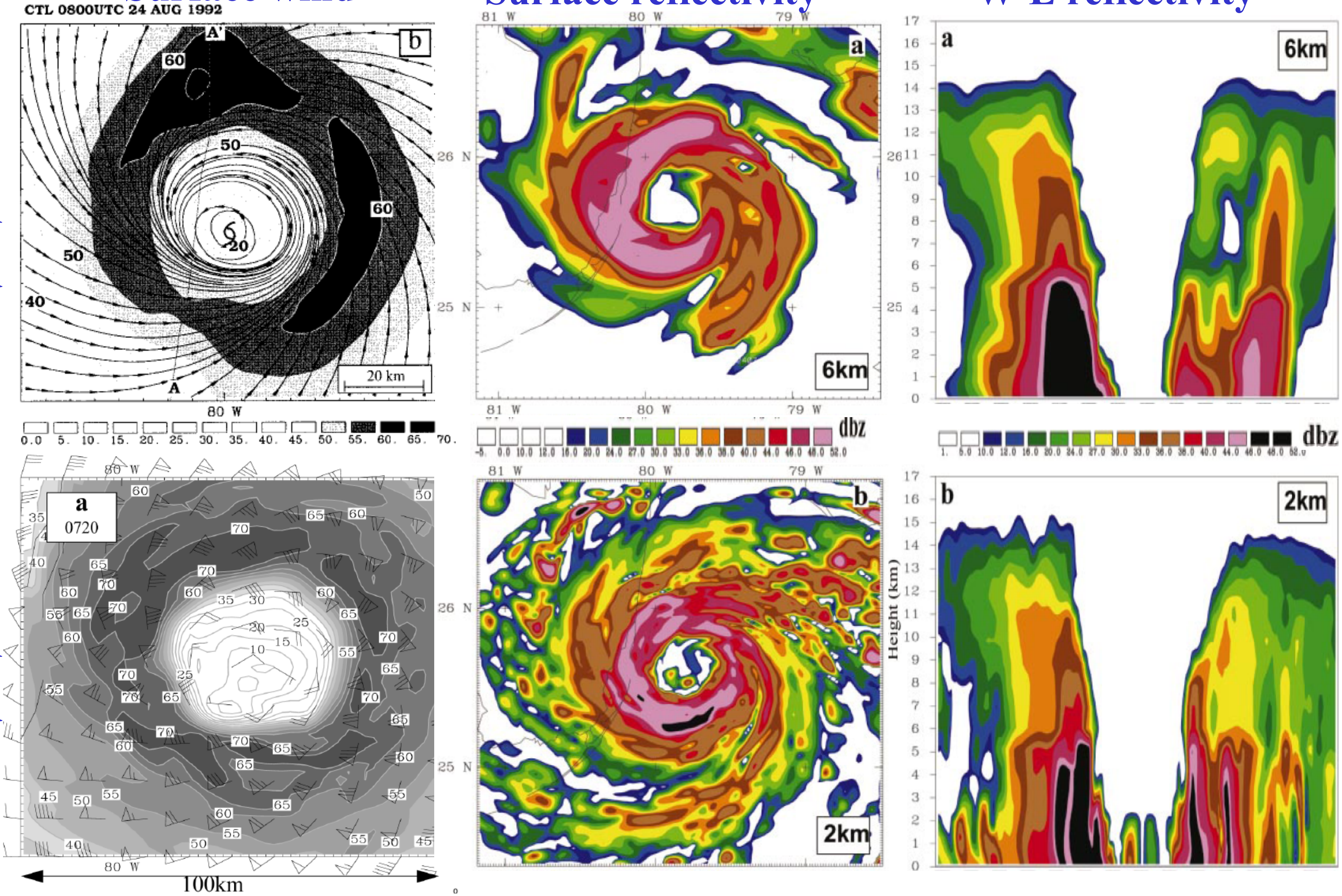

THE SECONDARY CIRCULATION
Airborne-Doppler Radar Observations

Rogers *et al.* 2012 :
Mon. Wea. Rev., 140, 77-99

The multiscale inner-core structure of mature tropical cyclones is presented via the use of composites of airborne Doppler radar analyses.

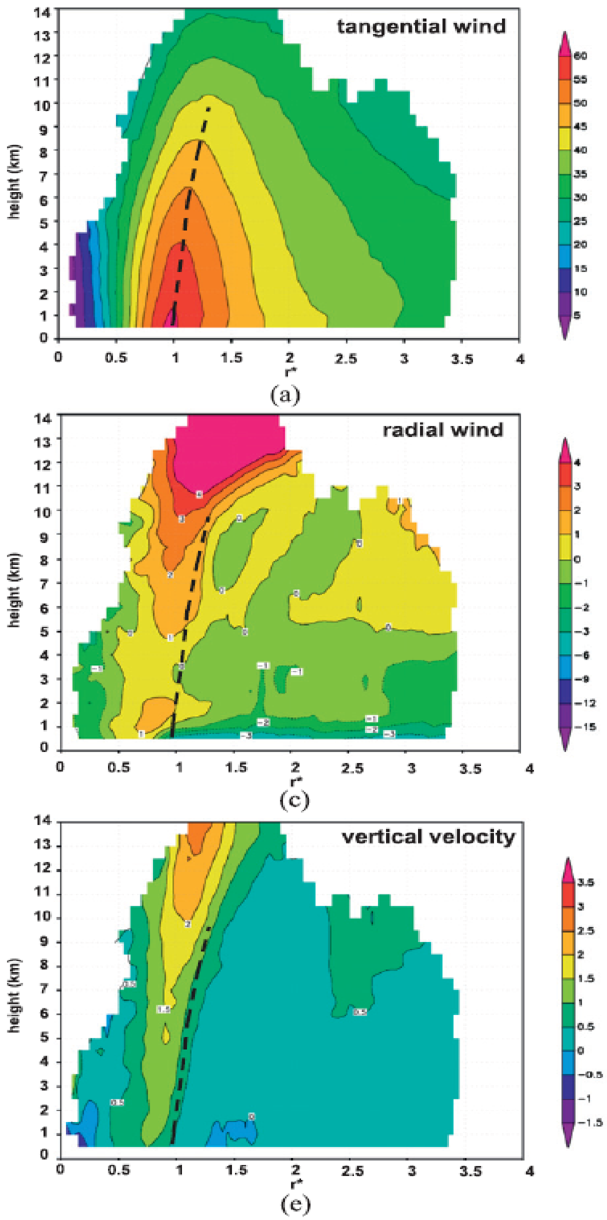

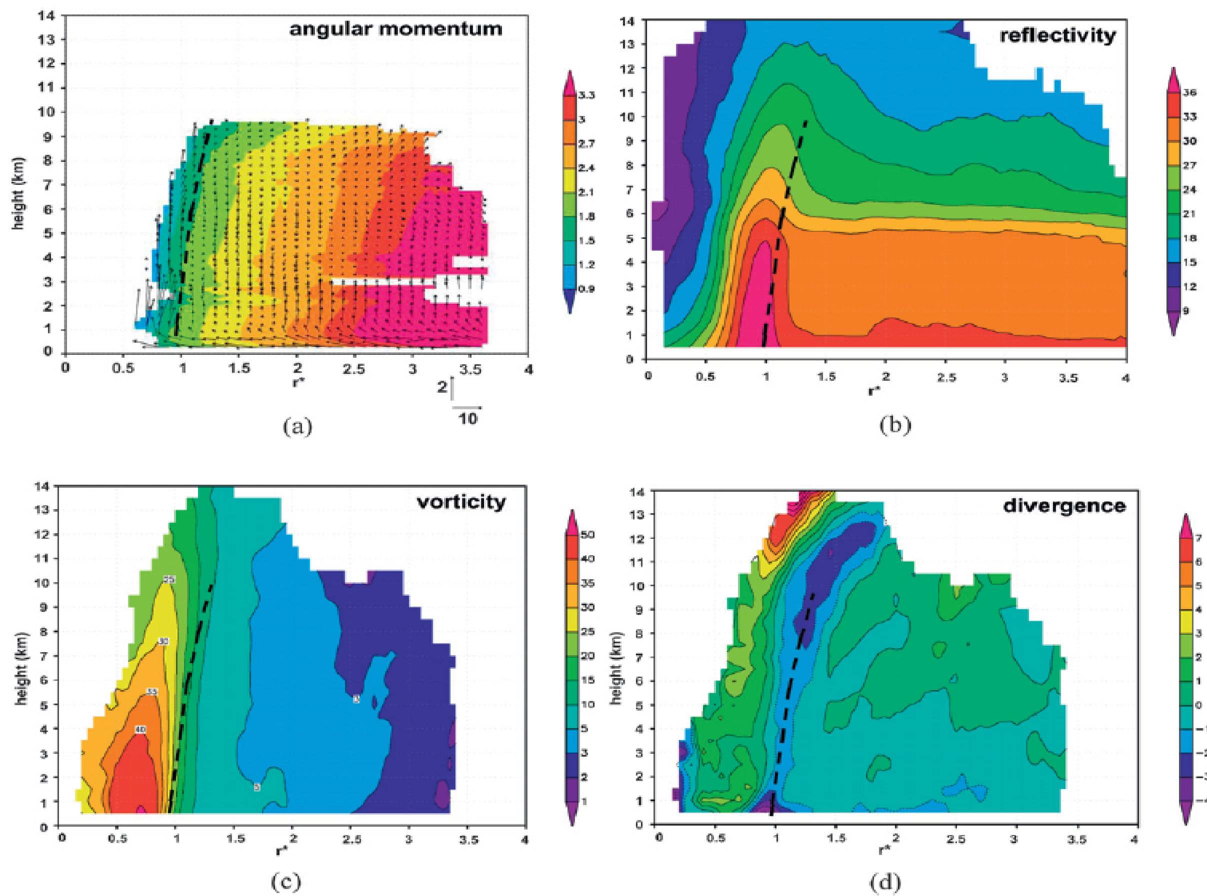

THE SECONDARY CIRCULATION : Microphysics (1)

Wang 2002a [*Mon. Wea. Rev.*, 130, 3022-3036]

→sensitivity of the simulated TC structure and intensity to the details of cloud microphysics parameterization : warm-rain only (WMRN), crystal-snow-graupel (CTRL), crystal-snow-hail (HAIL), no evaporation of rain (NEVP), no melting (NMLT)

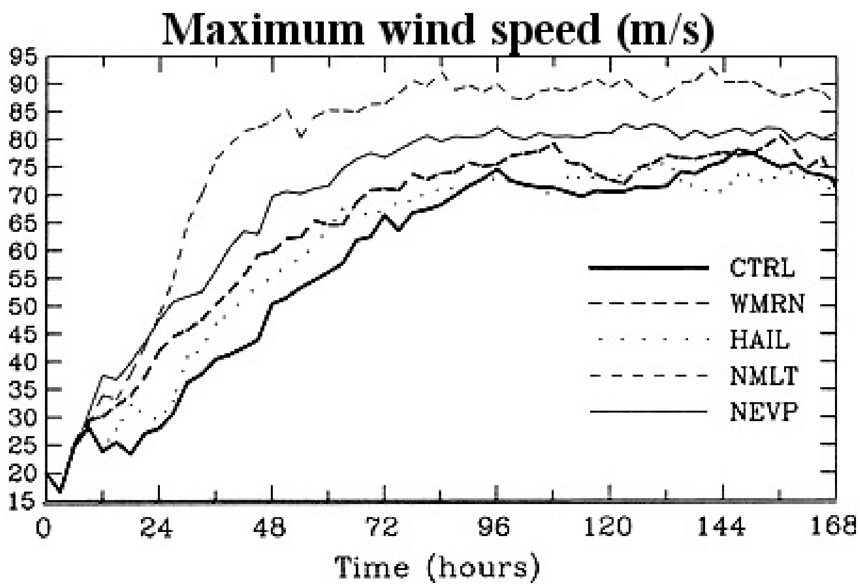

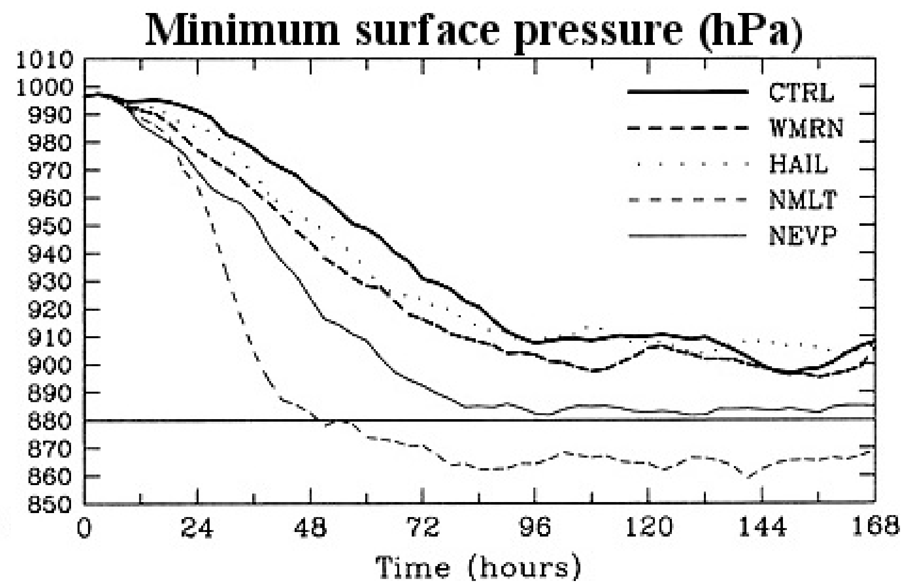

The simulated TC develops more rapidly and reaches a stronger intensity for « warm-rain only » , « no evaporation » and « no melting » experiments

THE SECONDARY CIRCULATION : Microphysics (2)

Vertical cross-section of reflectivity

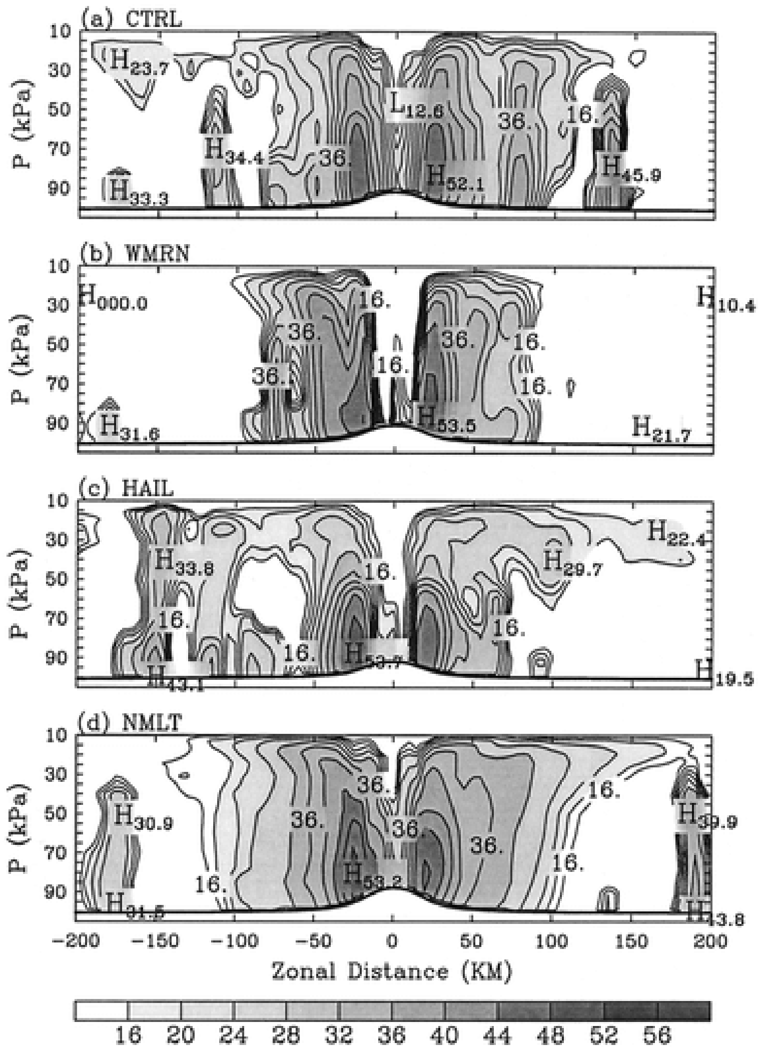

Surface reflectivity in 360 km x 360 km

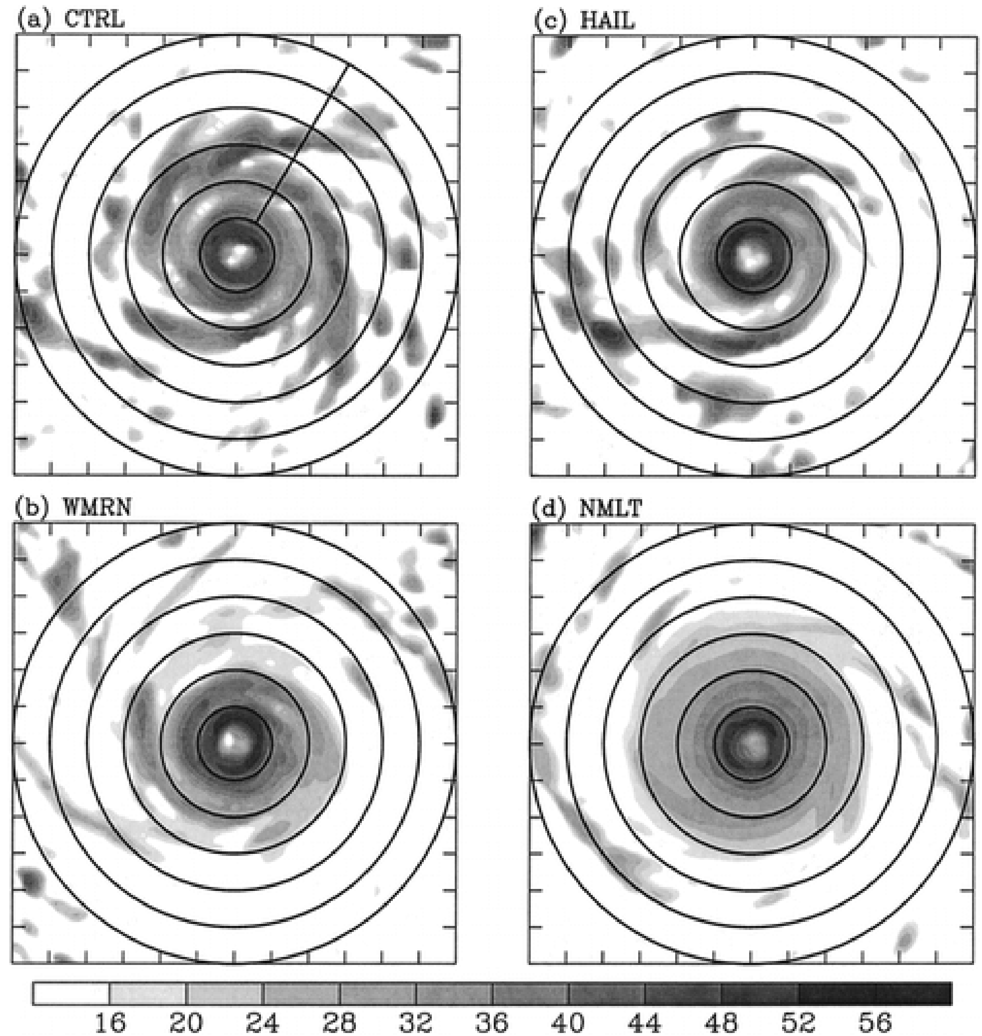

THE SECONDARY CIRCULATION : Microphysics (3)

Tao *et al.* 2011 :
Asia-Pacific J. Atmos. Sci., 47, 1-16

Simulation of Hurricane Katrina (2005) with the triple-nested (15, 5 and 1.667 km) WRF model with <u>six different microphysical schemes</u> (<u>including the ice phase</u>)

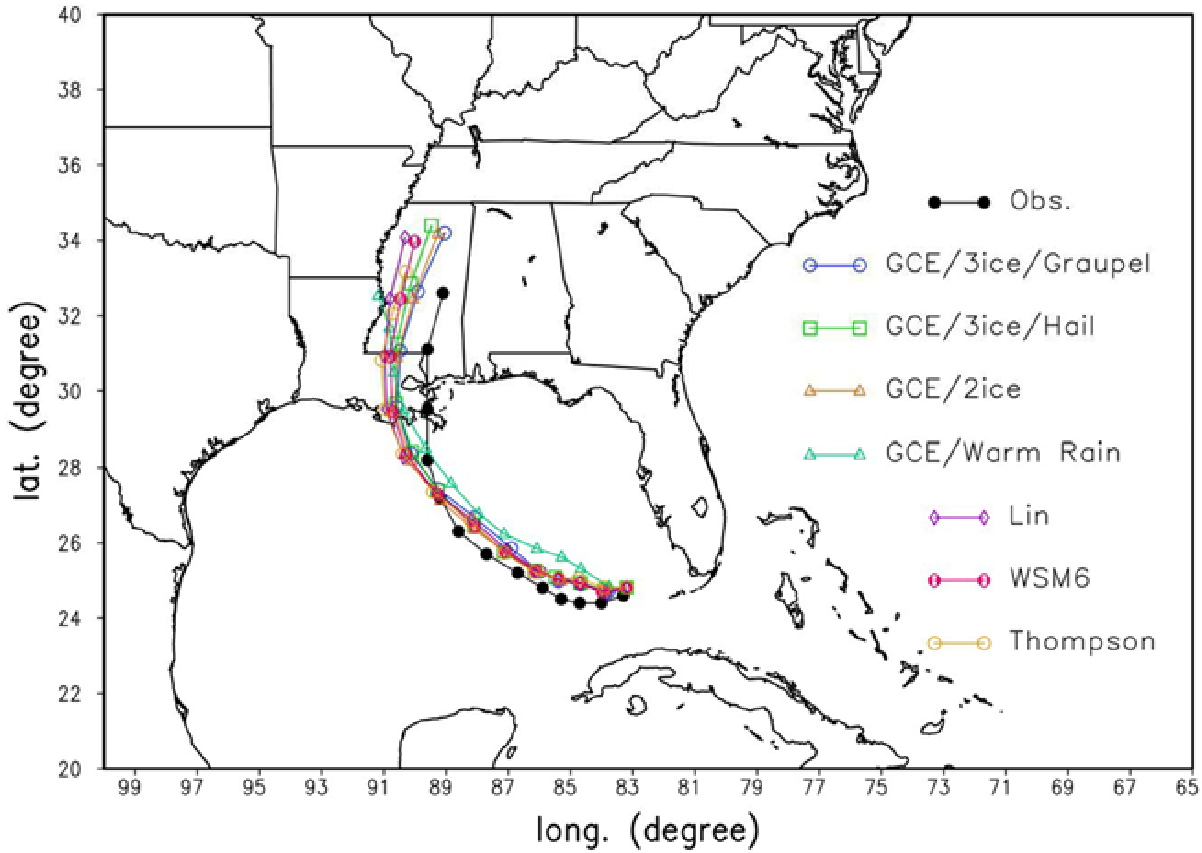

The sensitivity tests show <u>no significant difference in track</u> among the different microphysical schemes

THE SECONDARY CIRCULATION : Microphysics (4)

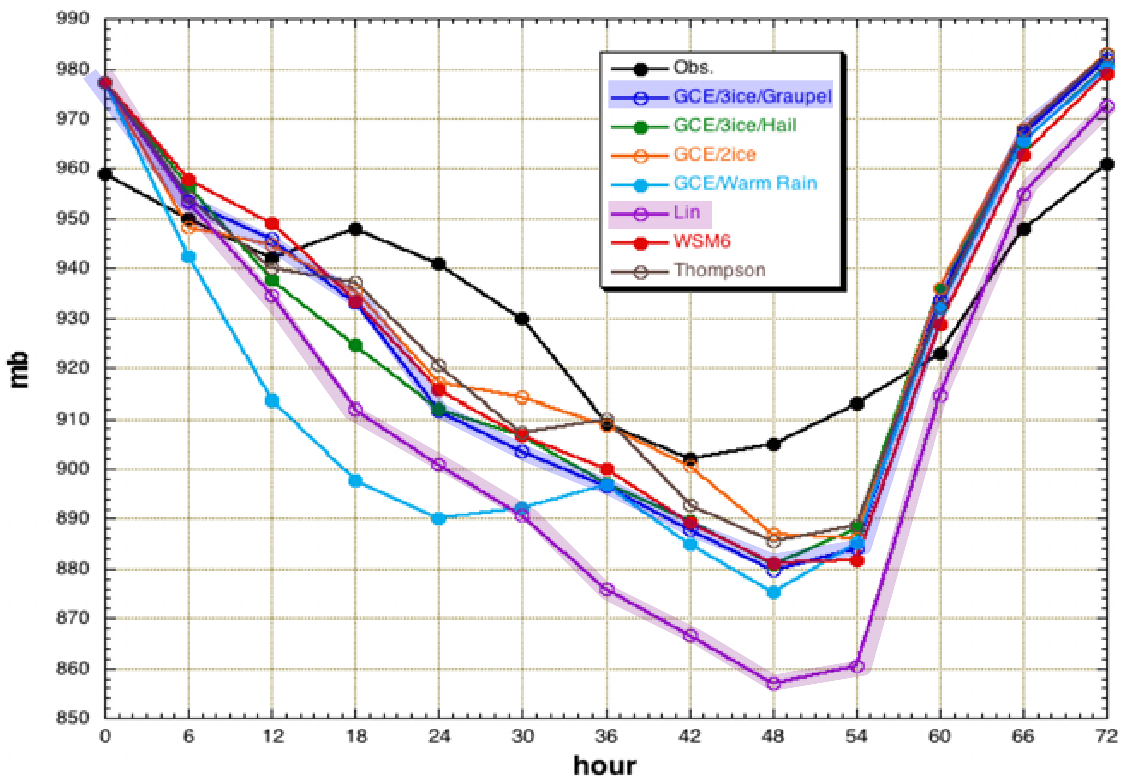

Minimum sea level pressure (hPa) obtained from WRF forecasts of Hurricane Katrina using six different microphysical schemes

	3ICE-Hail	3ICE-Graupel	2ICE	WSM6	Lin	Thompson
Liquid hydrometeor	46.6%	36.4%	24.8%	50.4%	65.3%	34.2%
Solid Hydrometeor	53.4%	63.6%	75.2%	49.6%	34.7%	65.8%

Domain- and 72-h time-average accumulated liquid (warm rain) and solid (ice) water species for the Hurricane Katrina case.

THE SECONDARY CIRCULATION : Lightning (1)

Molinari *et al.* 1994 [*J. Geophys. Res.*, 99, 16665-16676]

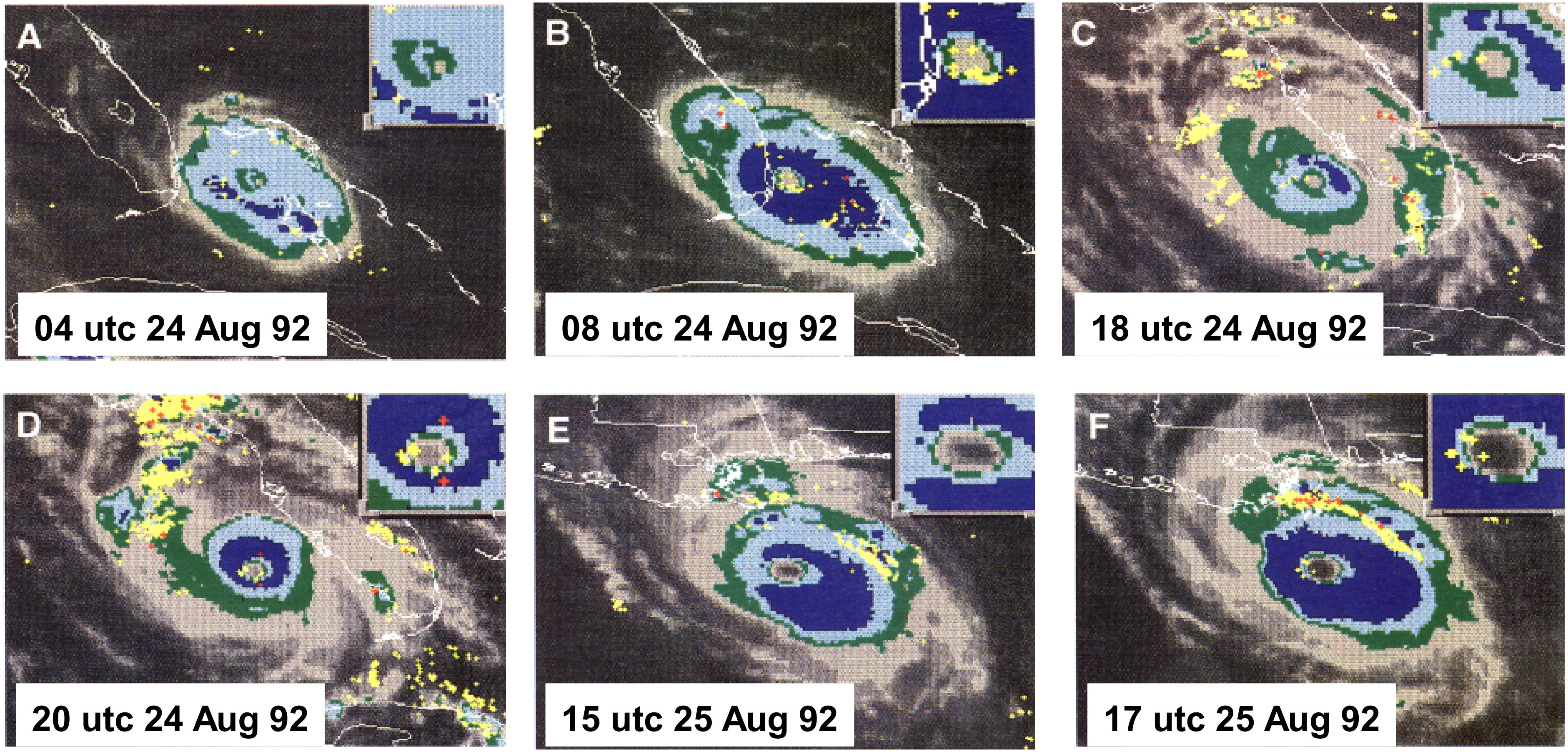

Variation of lightning in Hurricane Andrew, superimposed on infrared satellite images. The insets show a 2× view of the eye and eyewall.

THE SECONDARY CIRCULATION : Lightning (2)

Molinari *et al.* 1999 [*Mon.Wea. Rev.*, <u>127</u>, 520-534]

Ground flash density (from NLDN) for 9 Atlantic hurricanes :

- <u>weak maximum in the eyewall</u> region (<u>before/during intensification</u>)

  →*weakly electrified « oceanic monsoonal convection »*
- <u>minimum 80-100 km outside the eyewall</u> (positive flashes)

  →*« mostly stratiform » precipitation*
- <u>strong maximum in outer rainbands</u> (200-300 km radius)

  →*more convective*

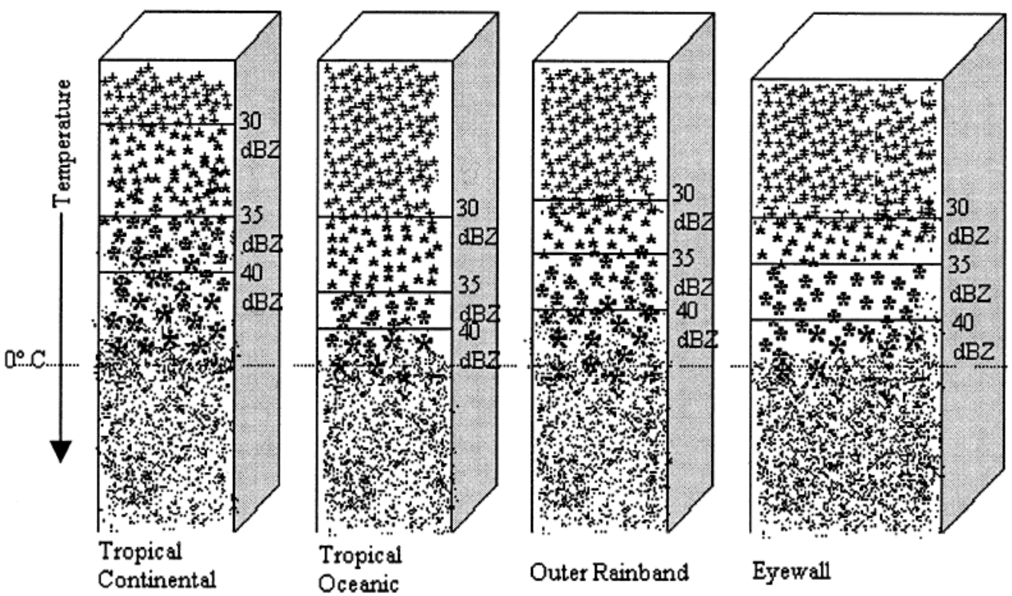

<u>Dots</u> indicate *liquid hydrometeors* ;
<u>Stars</u> indicate *frozen hydrometeors* with increasing symbol size representing larger graupel or hail.

Cecil & Zipser 2002 :
Mon. Wea. Rev., <u>130</u>, 785-801

THE SECONDARY CIRCULATION : Lightning (3)

Fierro *et al.* 2007 [*Meteor. Atmos. Phys.*, 98, 13-33]

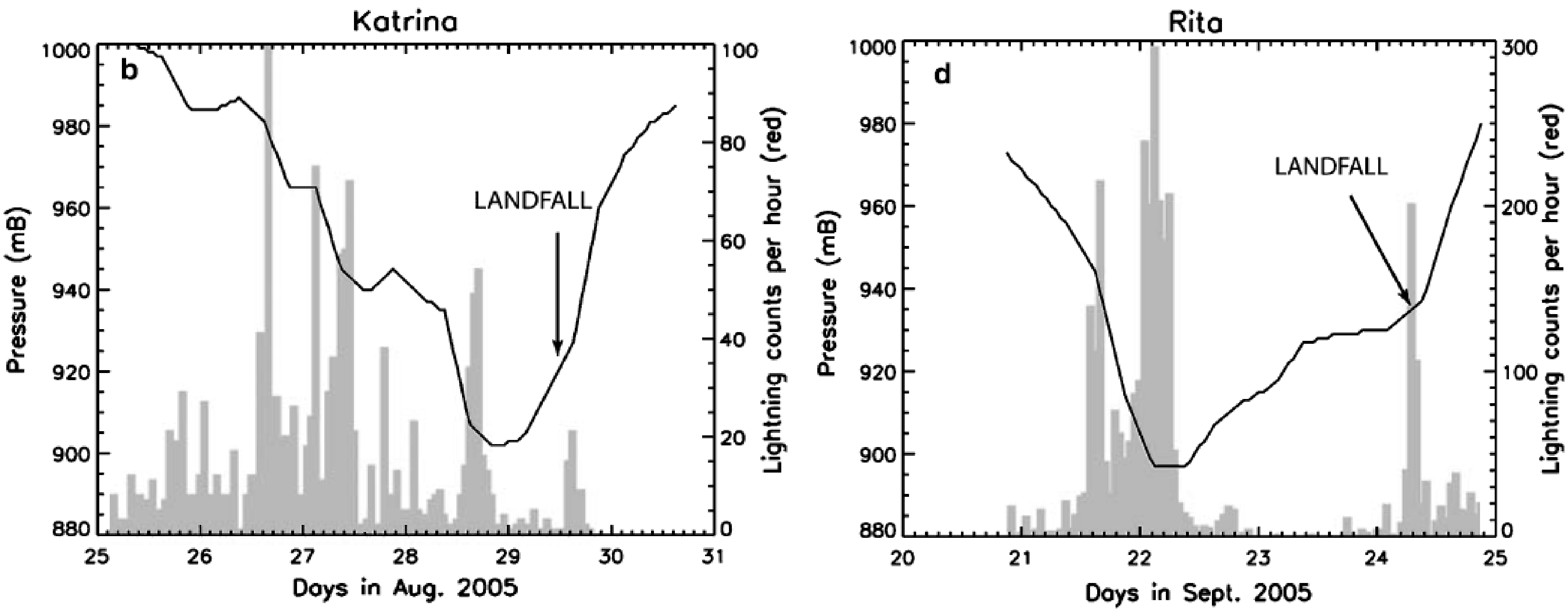

Hourly eyewall total lightning flash rate detected for Hurricanes Katrina and Rita of 2005 by LASA (Los Alamos National Laboratory's Sferic Array)
→ The eyewall lightning outbreaks might be a useful forecast tool to predict changes in hurricane intensity and therefore to diagnose storm intensification.

THE SECONDARY CIRCULATION :
« Convective » Sources and « Thermal Wind » Balance

Willoughby *et al.* 1982
J. Atmos. Sci., 39, 395-411

Heat source

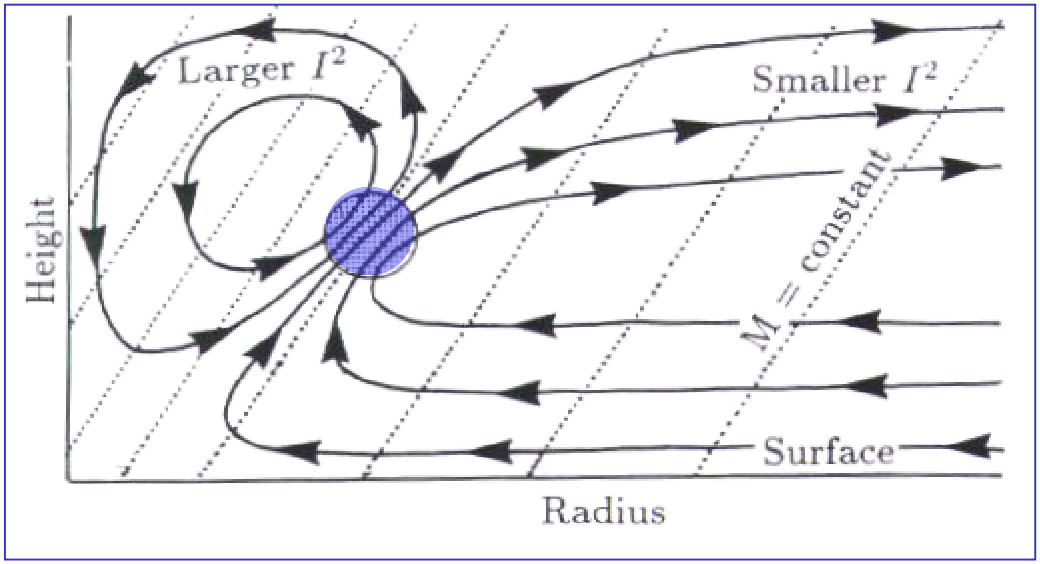

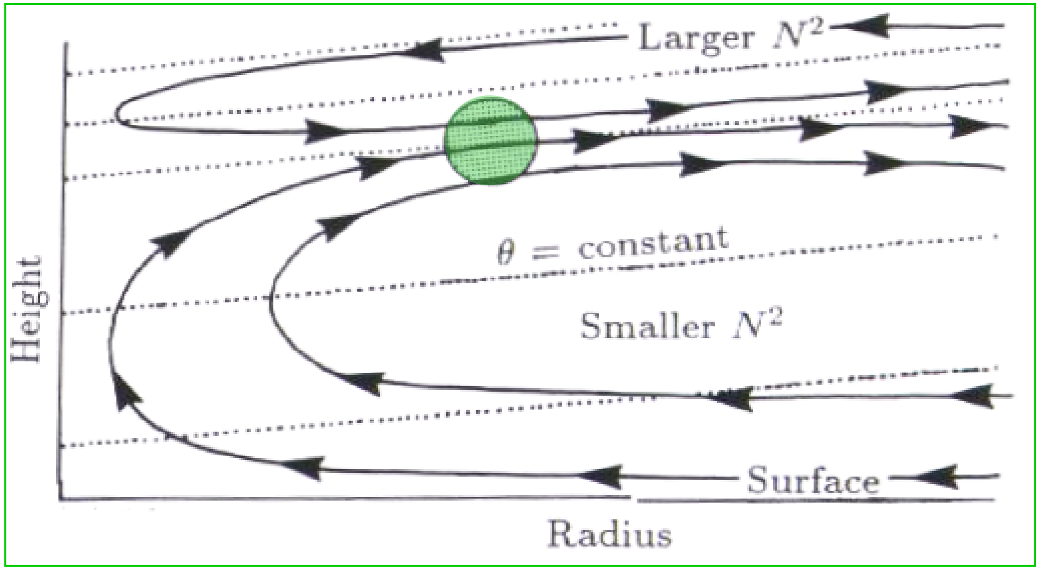

Momentum source

THE SECONDARY CIRCULATION : Evolution

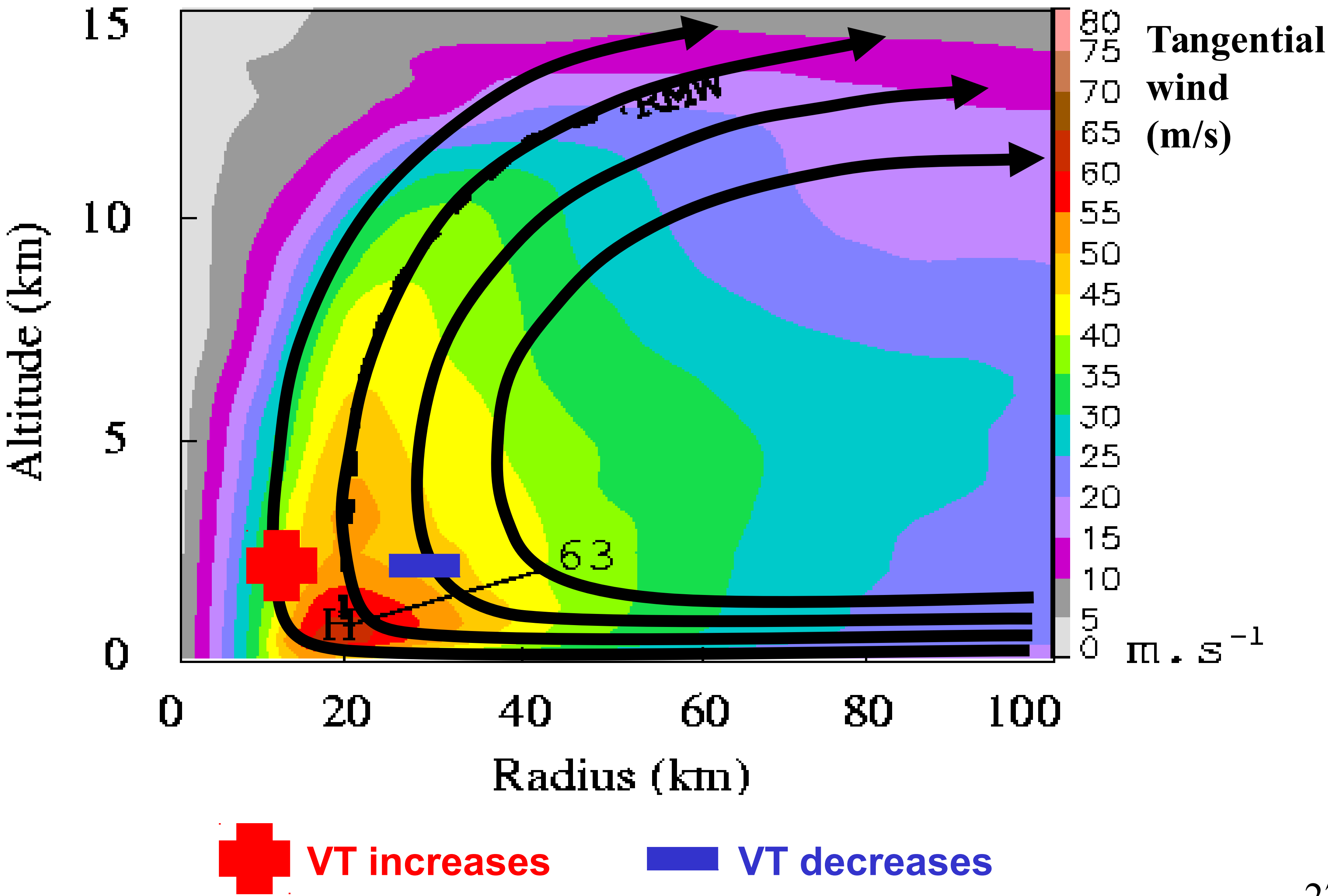

THE SECONDARY CIRCULATION :
Eyewall Replacement Cycle (1a)

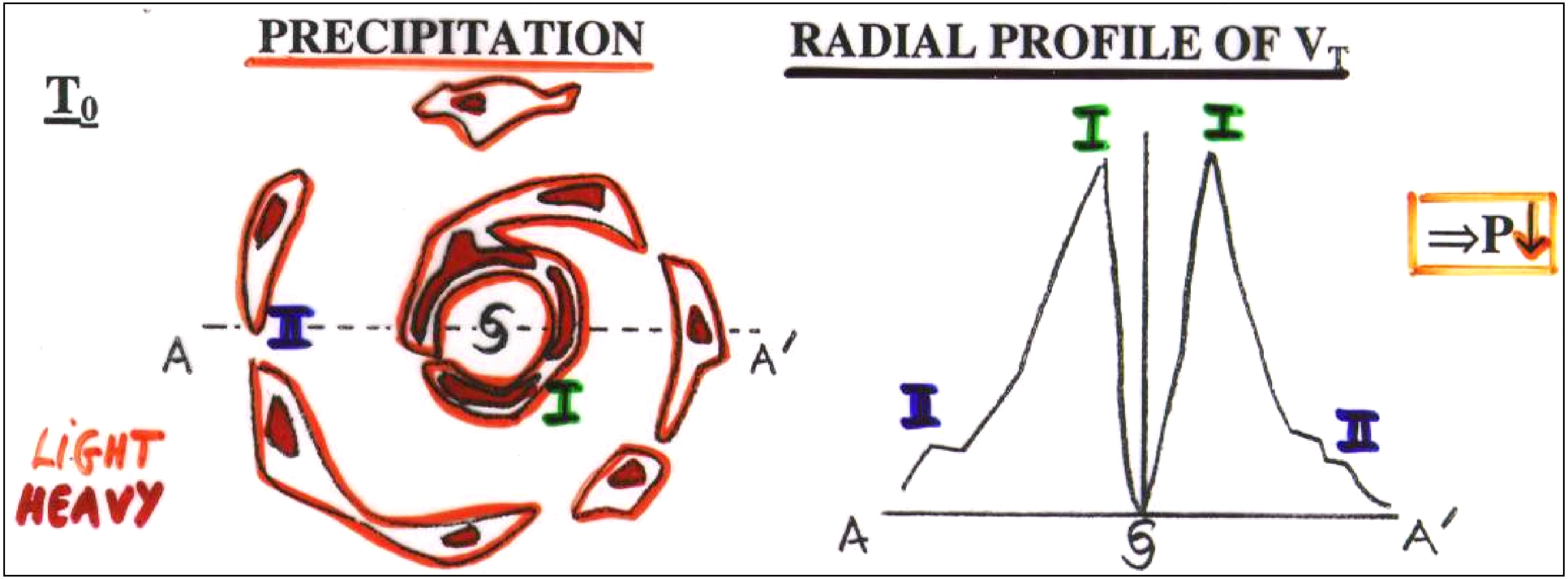

THE SECONDARY CIRCULATION :
Eyewall Replacement Cycle (1b)

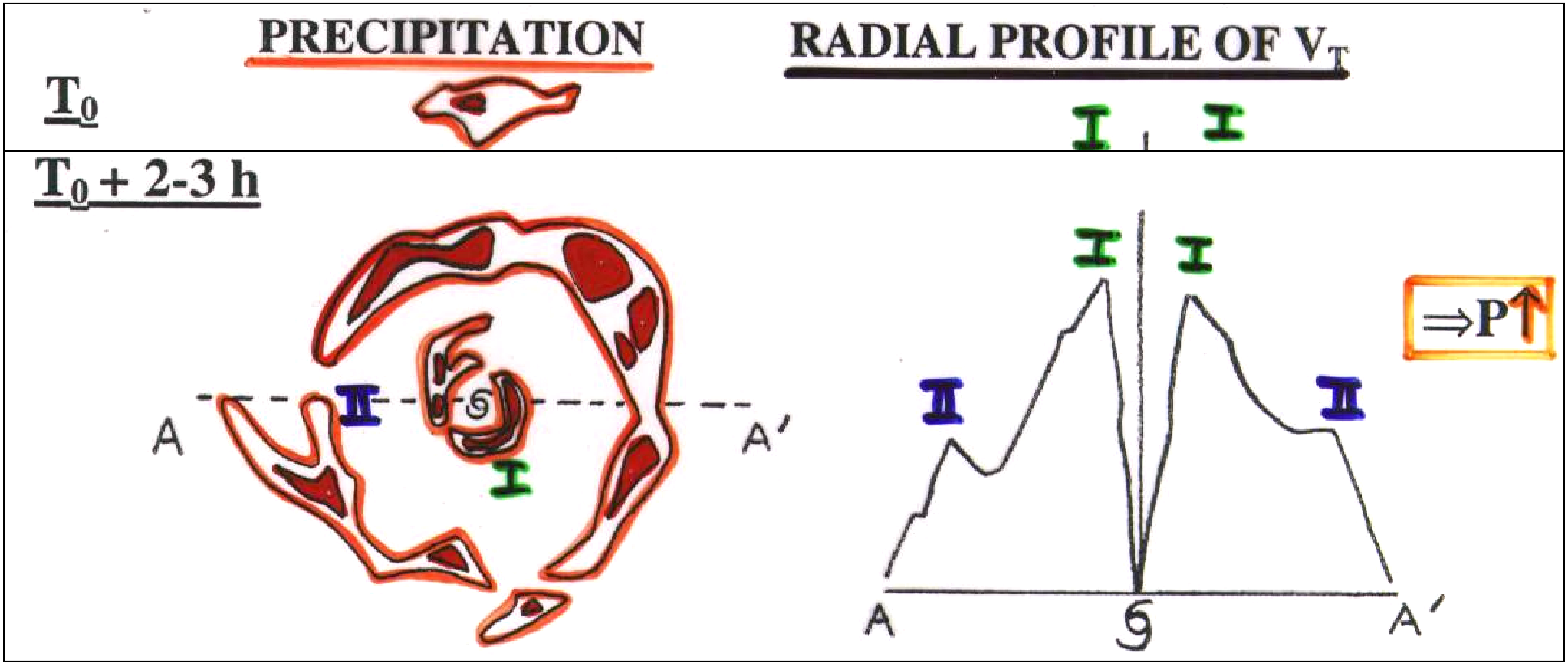

THE SECONDARY CIRCULATION :
Eyewall Replacement Cycle (1c)

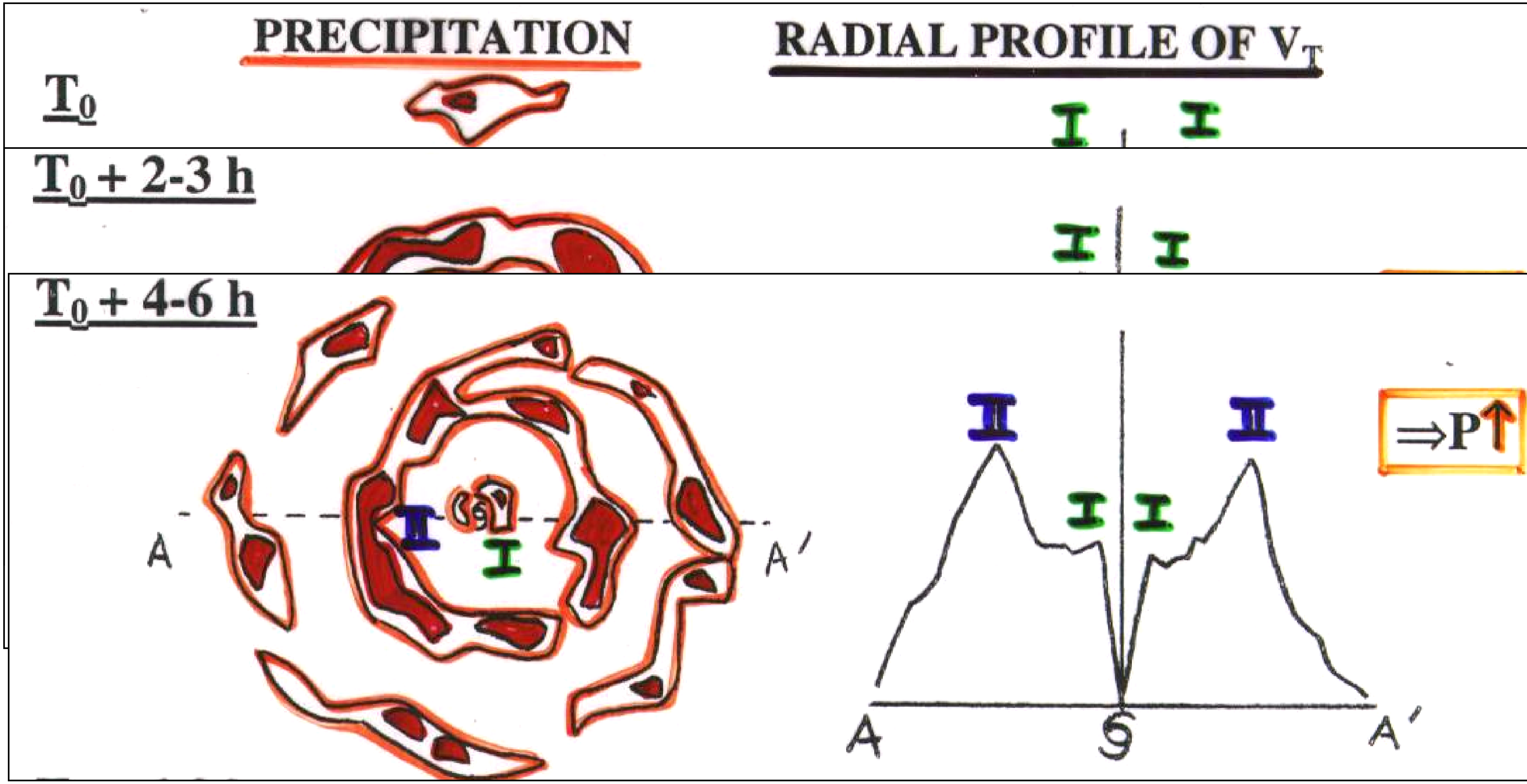

THE SECONDARY CIRCULATION :
Eyewall Replacement Cycle (1d)

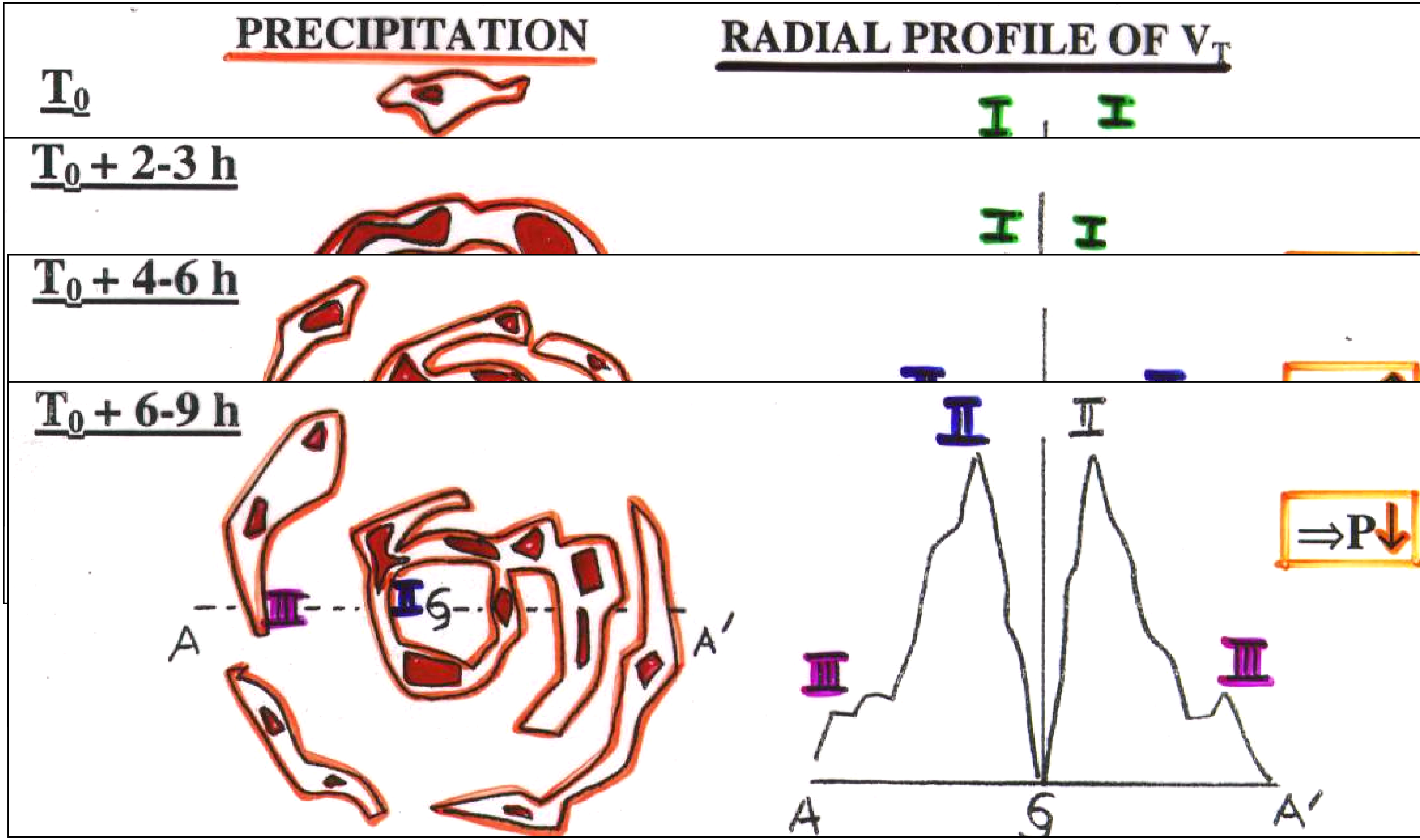

THE SECONDARY CIRCULATION :
Eyewall Replacement Cycle (2)

Hurricane Intensity and Eyewall Replacement
Robert A. Houze, Jr., *et al.*
Science **315**, 1235 (2007); **RAINEX (2005)**

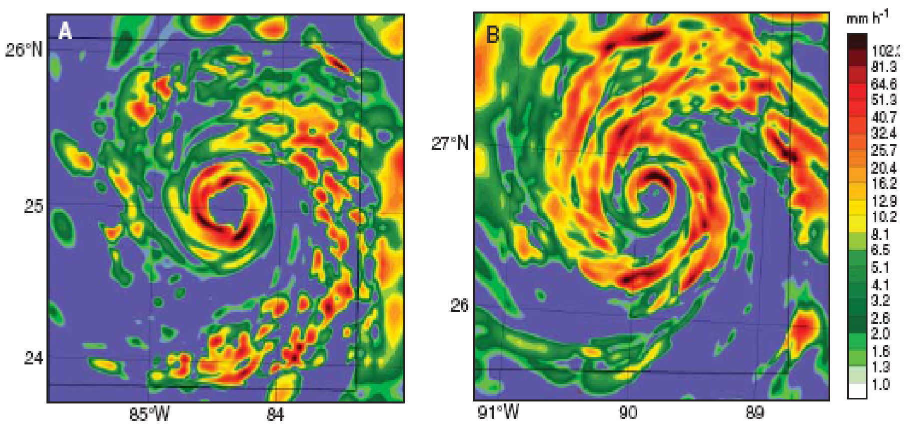

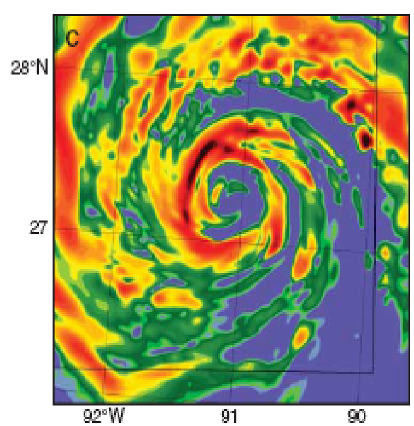

Fig. 1. Forecast of surface rainfall intensity in Hurricane Rita. (**A**) 0715 UTC 21 September, (**B**) 1115 UTC 22 September, (**C**) 1715 UTC 22 September. Colors show the rainfall rate (mm h^{-1}) at the sea surface generated by the University of Miami's high-resolution, vortex-following, coupled atmosphere-wave-ocean version of the fifth-generation Pennsylvania State University/ NCAR nonhydrostatic mesoscale model (MM5) (*34*) operating at a horizontal resolution of 1.67 km. Initial fields at 0000 UTC 20 September 2005 and lateral boundary conditions are from the NOGAPS global numerical forecast model (*35*).

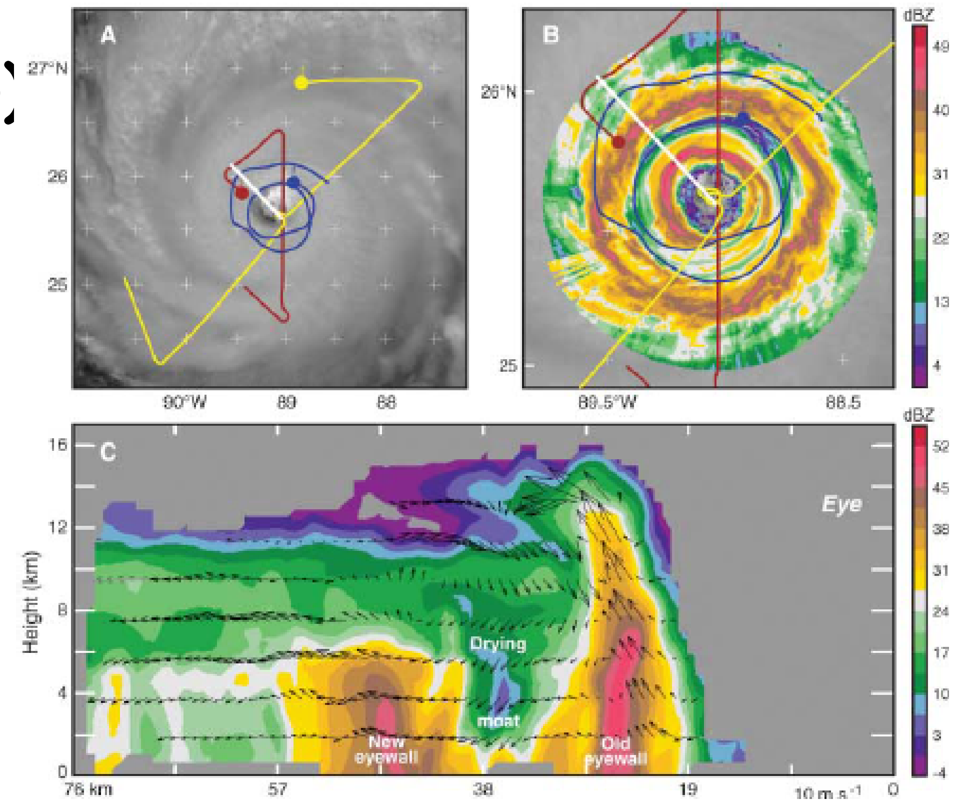

Fig. 2. Aircraft data collected in Hurricane Rita between 1800 and 1820 UTC 22 September 2005. (**A**) and (**B**) are plan views; (**C**) is a vertical cross section across the northwest side of the storm (along the white line in the plan views). Colored lines in (A) denote the flight tracks of the three RAINEX aircraft: yellow and red are the NOAA aircraft tracks; blue is the NRL aircraft, which was instrumented with ELDORA. The dots show aircraft locations as of 1830 UTC. The yellow track segment is for the 80 min preceding that time; the red and blue track segments are for the preceding 45 min. The yellow NOAA track was part of a wide pattern to determine the broad-scale structure of the cyclone vortex. The red NOAA track was part of an intermediate pattern, with shorter legs across the center of the storm to monitor the two eyewalls. The blue NRL track was the circumnavigation that obtained the key radar and sounding data referred to in this article. The

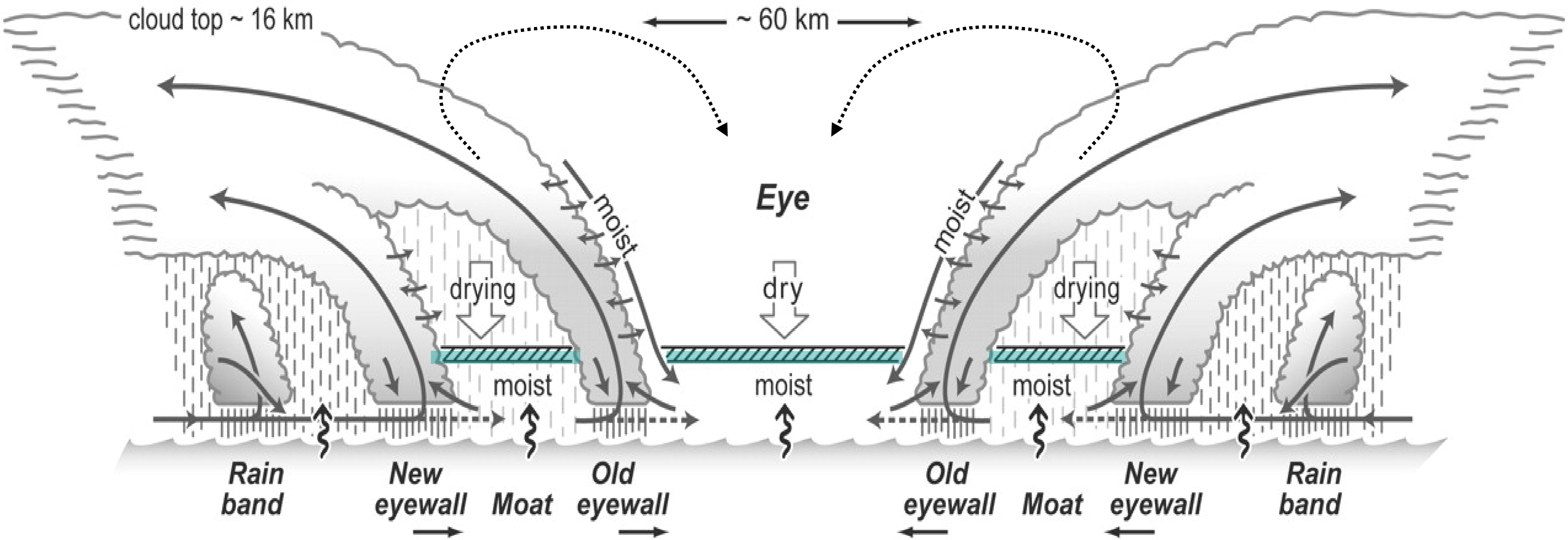

Two interacting eyewalls, separated by the moat, were contracting inward.

- The vertical lines below the clouds indicates precipitation ;
- Thin arrows show the direction of air motion relative to the storm. Dashed segments indicate partially interrupted flow ;
- Wavy arrows at the sea surface indicate upward water vapor flux ;
- The broad arrows indicate the dry downward motion in the eyewall ;
- The hatched zone shows the top of the near-surface moist layer, which is capped by the stabilizing and drying effect of subsiding air above.

EXTERNAL RAINBANDS (1)

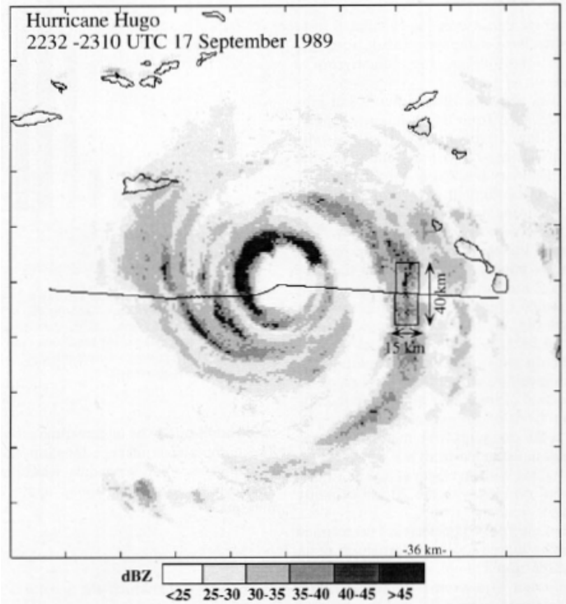

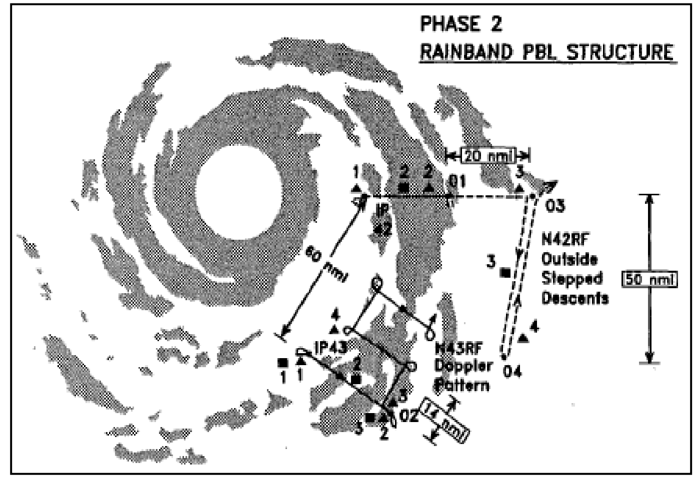

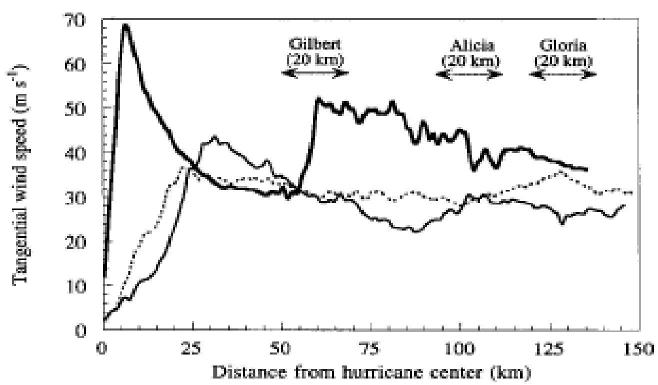

FIG. 2. Storm-relative tangential wind profiles of Hurricane Gilbert from 1012 to 1029 UTC 14 September 1988 (bold, solid line), Hurricane Alicia from 1352 to 1413 UTC 17 August 1983 (thin, solid line), and Hurricane Gloria from 1932 to 1951 UTC 26 September 1985 (thin, dashed line). The three shaded regions delineate the 20

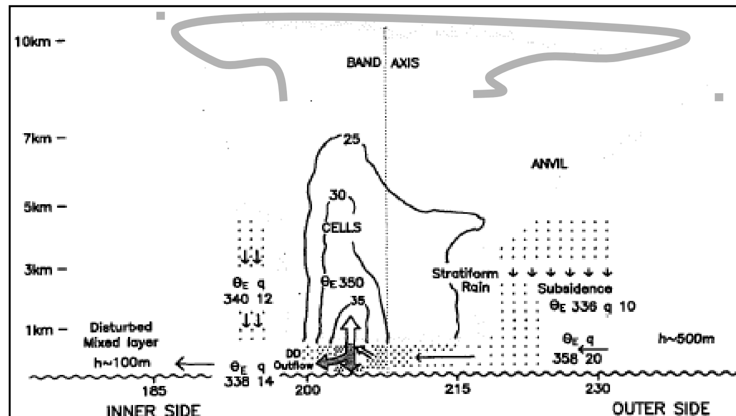

FIG. 14. Schematic cross section of the thermodynamic structure in the Hurricane Earl rainband. Outer solid contour indicates band cloud edges while other contours represent radar reflectivity. Horizontal arrows represent crossband component of the wind, bold vertical arrows indicate convective core updrafts and downdrafts, small downward arrows indicate mesoscale subsidence regions and larger downward arrows indicate penetrative downdrafts originating in the inner anvil region.

Samsury & Zipser 1995 [*Mon. Wea. Rev.*, 123, 3502-3517] ≈30% of the external rainbands show a secondary maximum in tangential wind

Powell 1990 [*Mon. Wea. Rev.*, **118**, 891-938] local convective donwdrafts reduce θ_E in the low levels

EXTERNAL RAINBANDS (2)

Wang 2001 [*Mon. Wea. Rev.*, 129, 1370-1394]

Triply-nested, 2-way interactive, movable mesh model using hydrostatic primitive equations, with explicit « liquid+ice » microphysics, initialized with an axisymmetric vortex embedded in uniform easterly flow of 5 m/s on a « f-plane »

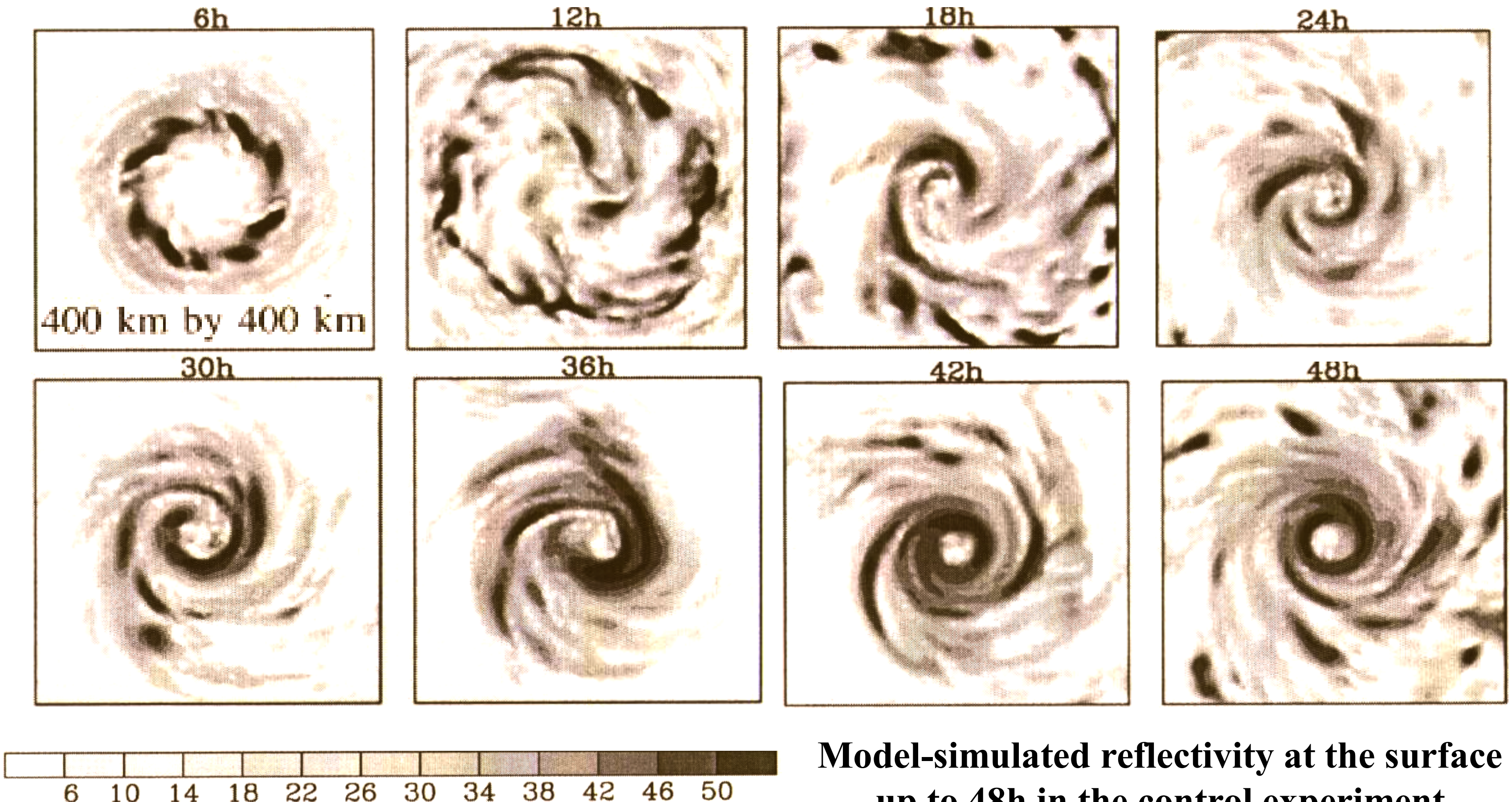

Model-simulated reflectivity at the surface up to 48h in the control experiment

EXTERNAL RAINBANDS (3)

Reasor *et al.* 2000 [*Mon. Wea. Rev.*, 128, 1653-1680]

An azimuthal wavenumber-2 feature dominates the asymmetry in relative vorticity below 3 km height in hurricane Olivia (1994) (*from reflectivity and wind composites from airborne Doppler radar data*)

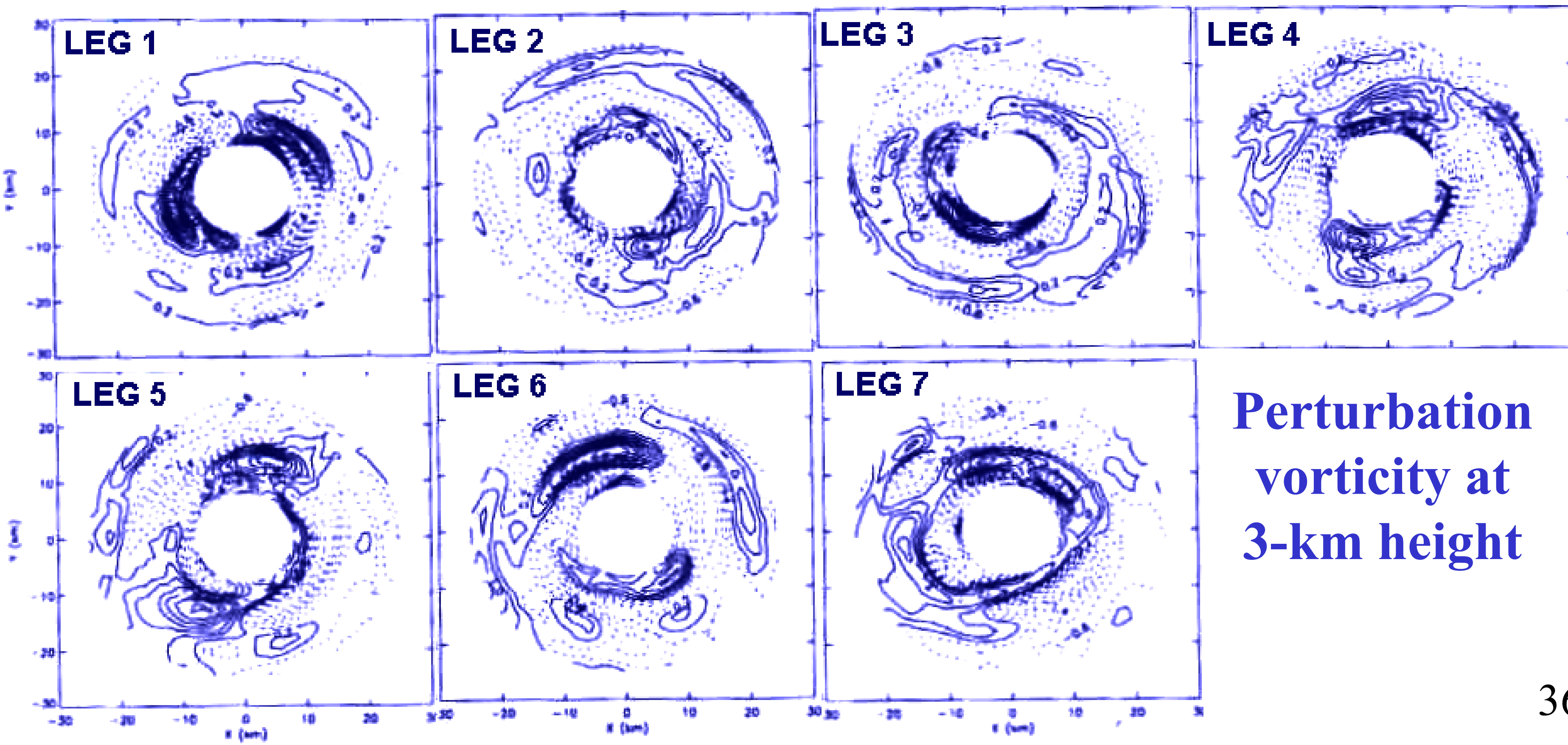

Perturbation vorticity at 3-km height

EXTERNAL RAINBANDS (3)

Romine & Wilhelmson 2006 [*Mon. Wea. Rev.*, 134, 1121-1139]

TABLE 1. Summary of hypotheses that have been proposed to explain the formation of core and outer spiral rainbands within hurricanes. Small-scale bands are defined as observed bands that have ~10 km horizontal scale.

Case	Proposed banding mechanism	Brief description	Comments
1	Inertia-buoyancy waves (Kurihara 1976)	Outward-propagating disturbance excited by eyewall convection	Three gravity wave modes, all with horizontal scales much larger than small-scale bands (25–200 km)
2	Inertia-buoyancy waves (Willoughby 1977)	Outward-propagating disturbance excited by eyewall convection	Favored horizontal scale ~20 km
3	Inertia-buoyancy waves (Willoughby 1978)	Inward- and outward-propagating Eliassen–Palm waves	Unrealistic phase speeds relative to observations, large variation in proposed horizontal scale with radius
4	Rayleigh instability (Fung 1977)	Ekman shear–induced circulations in the boundary layer, outward propagating	20–60-km horizontal scale, increasing with radius, slow to stationary phase speed
5	Symmetric instability (Braun 2002)	Primarily attributed to eyewall convection	May act as a trigger mechanism for gravity or potential vorticity waves of varying scale
6	Boundary layer rolls (GTH98)	Outward propagating, driven by boundary layer shear with deep convection	Deep horizontal roll vortices, structure and propagation similar to small-scale bands
7	Boundary layer rolls (Wurman and Winslow 1998)	Shear parallel boundary layer rolls	Shallow roll vortices, over one order of magnitude smaller scale than small-scale bands, not suggested to cause rainbands
8	Potential vorticity waves (Montgomery and Kallenbach 1997)	Vortex shedding (outward) and/or potential vorticity source entrainment (inward)	Slow outward velocity and horizontal scale increasing with radius from center of 20–50 km
9	Kelvin–Helmholtz instability [Testud et al. (1980) based on mode III waves proposed by Lalas and Einaudi (1976)]	Propagating gravity wave mode generated under extreme shear conditions	Scale and propagation characteristics similar to small-scale bands, applied to rainbands associated with postfrontal precipitation

CIRCULATION IN THE EYE (1)

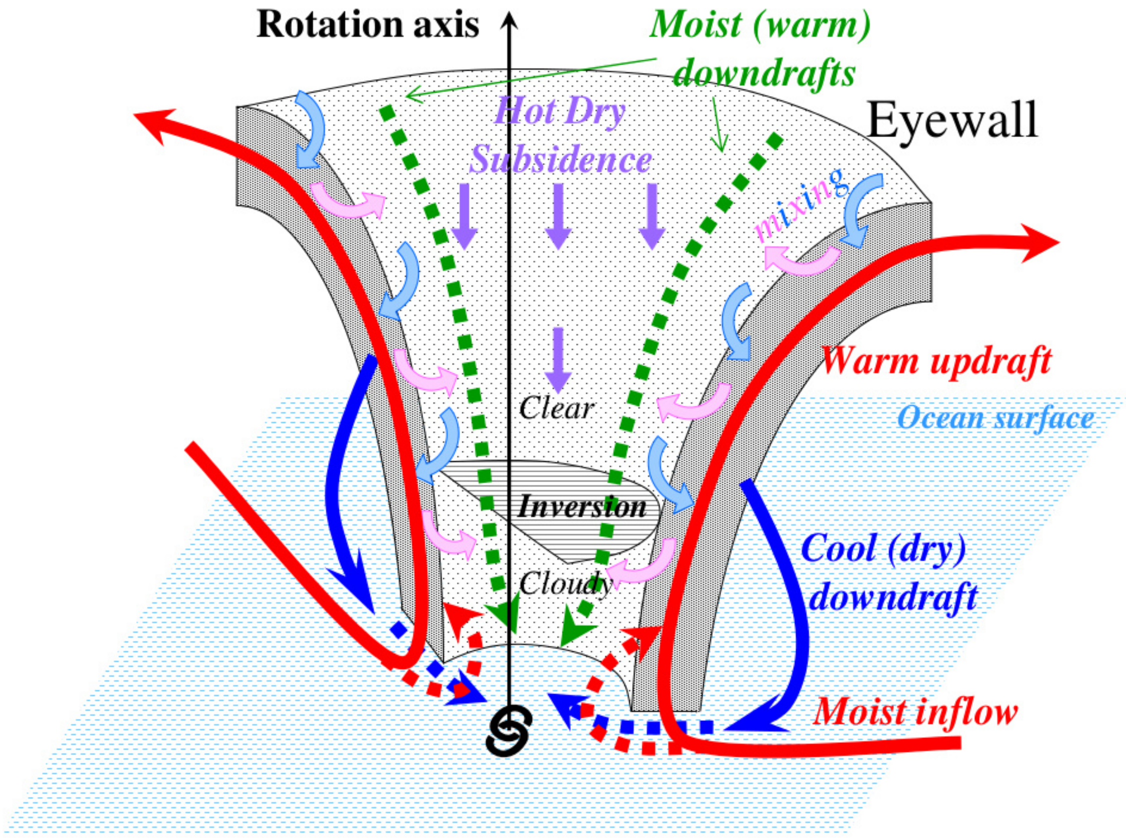

CIRCULATION IN THE EYE (2)

Category 5

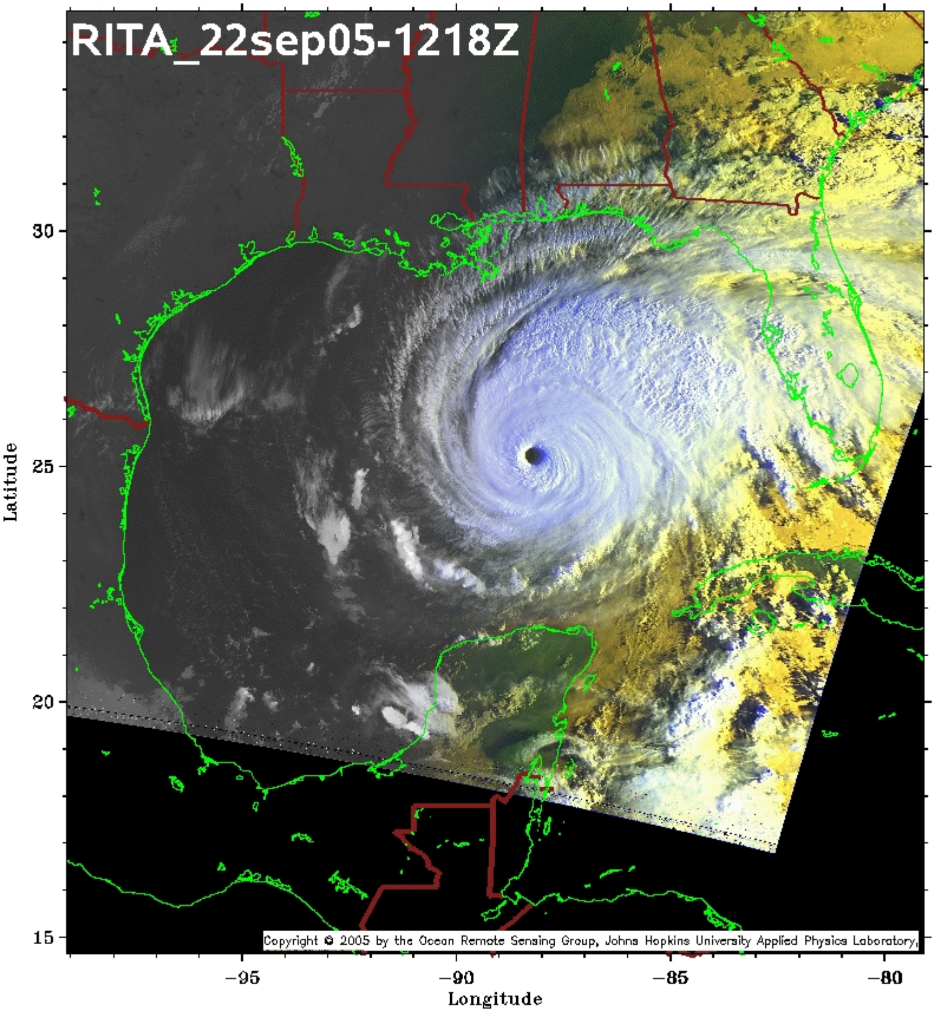

Category 3

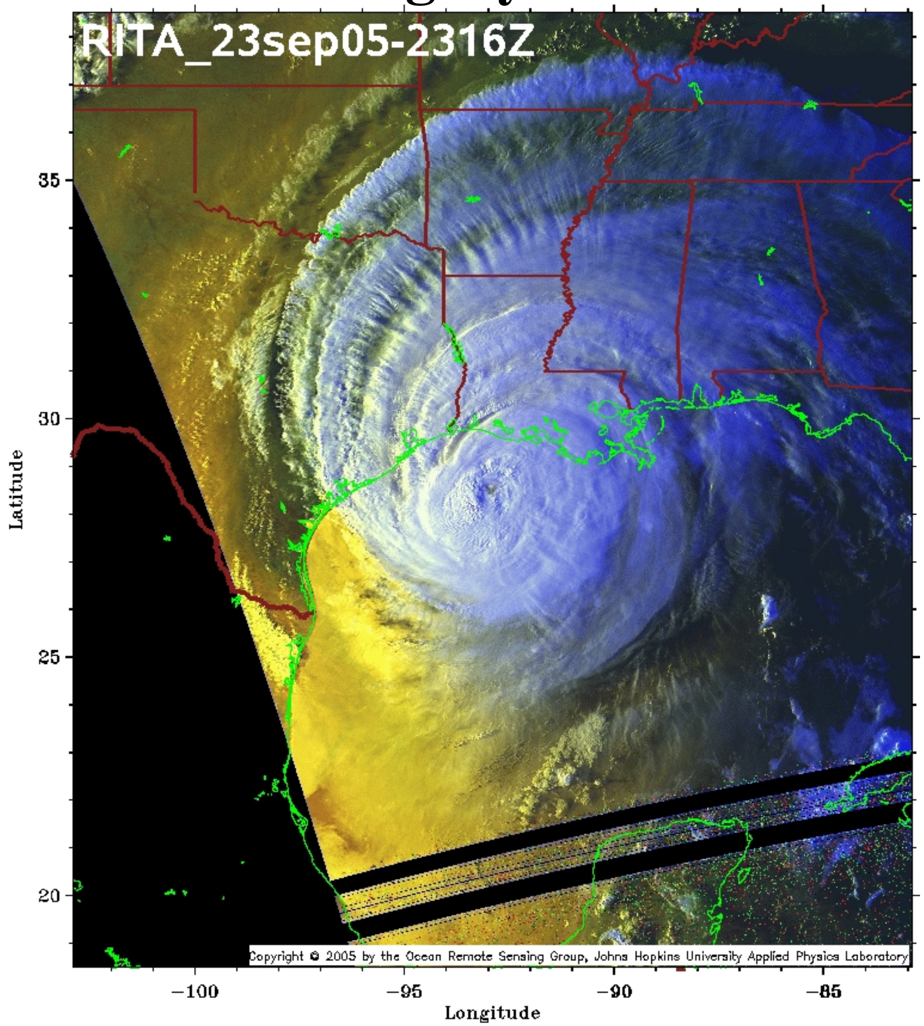

POLYGONAL EYEWALL (1)

Schubert *et al.*, 1999 [*J. Atmos. Sci.*, 56, 1197-1223]

Tropical cyclone eyewall occasionnally show polygonal (triangular to hexagonal) shapes. Other observations reveal the existence of intense « mesovortices » within or near the eye region.

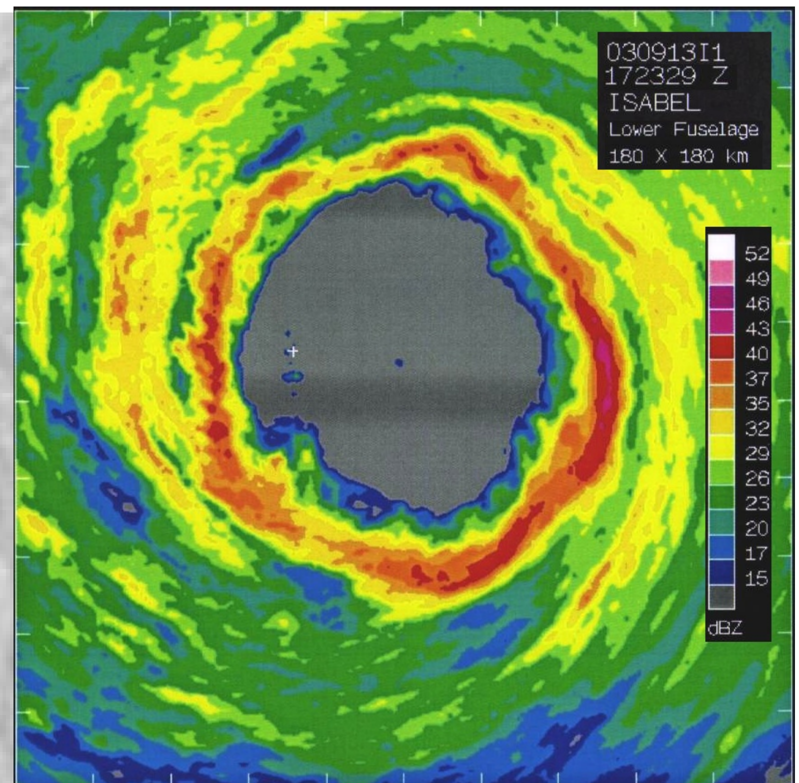

POLYGONAL EYEWALL (2)

Barotropic non-divergent model of 200 km x 200 km initialized with a ring of high PV in the eyewall, at some distance from the storm center.

When the instability grows to finite amplitude, the vorticity of the eyewall region pools into discrete areas, creating the appearance of polygonal eyewalls with embedded mesovortices.

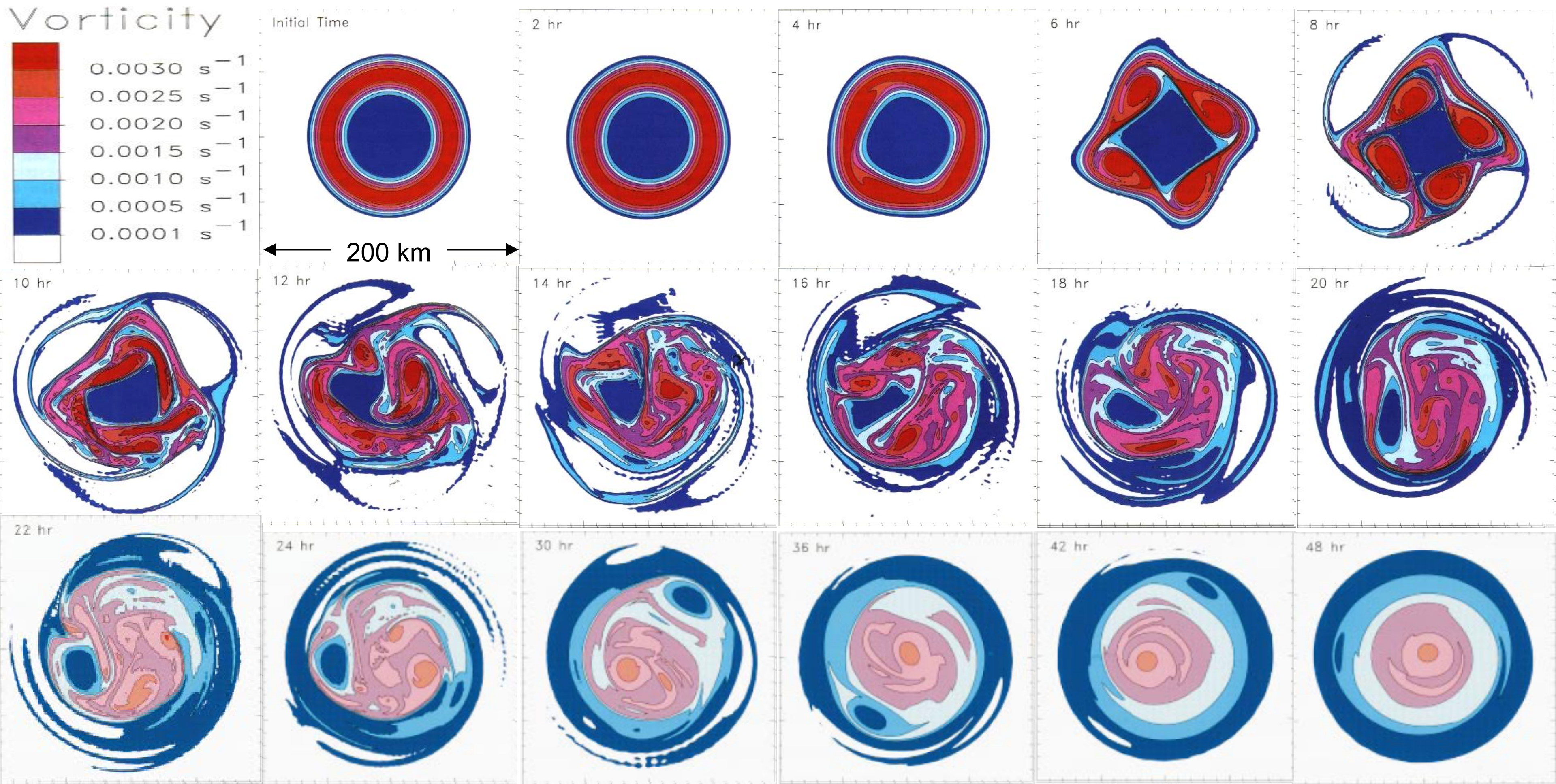

POLYGONAL EYEWALL (3)

Barotropic dynamics in the presence of both a cyclonic mean flow and a high PV gradient near the edge of the eye :

- the propagation of vortex Rossby waves in the cyclonic mean flow makes the eye rotate cyclonically
- the rotation period is longer that the period of advected parcels because the vortex Rossby waves propagate upwind

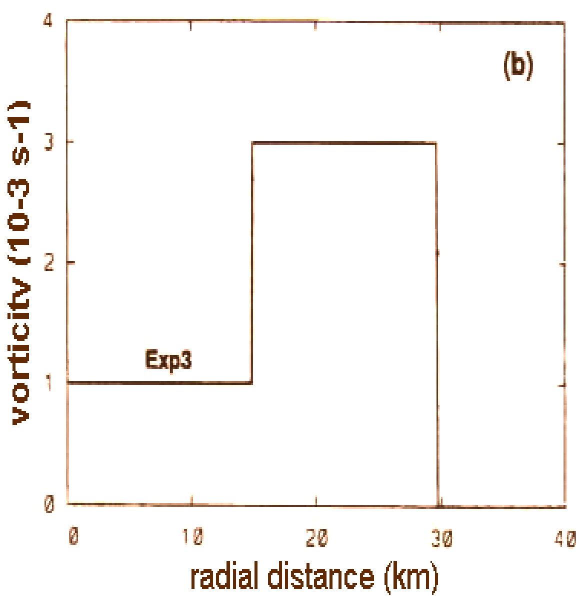

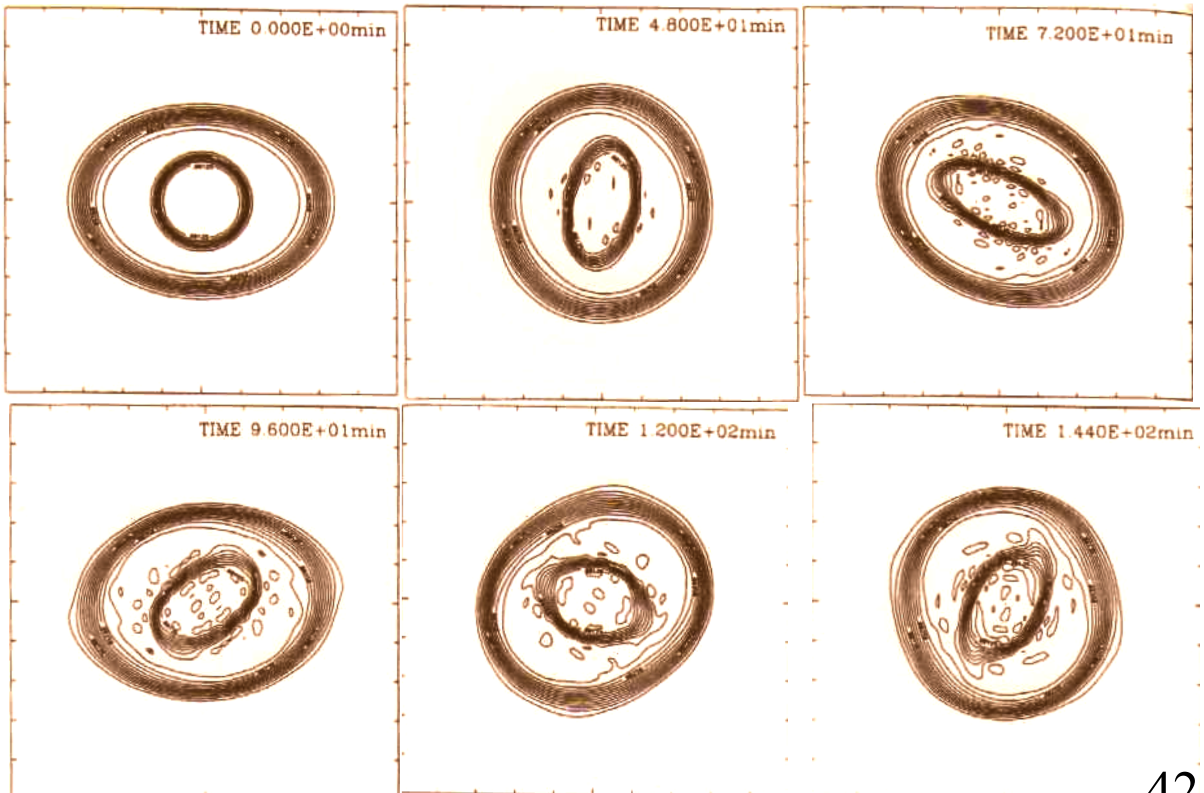

POLYGONAL EYEWALL (4)

Kuo *et al.* 1999 [*J. Atmos. Sci.*, 56, 1659-1673]

The elliptical eye of typhoon Herb (1996) with a semi-major axis of 30 km and a semi-minor axis of 20 km rotated cyclonically with a period of ≈145 min

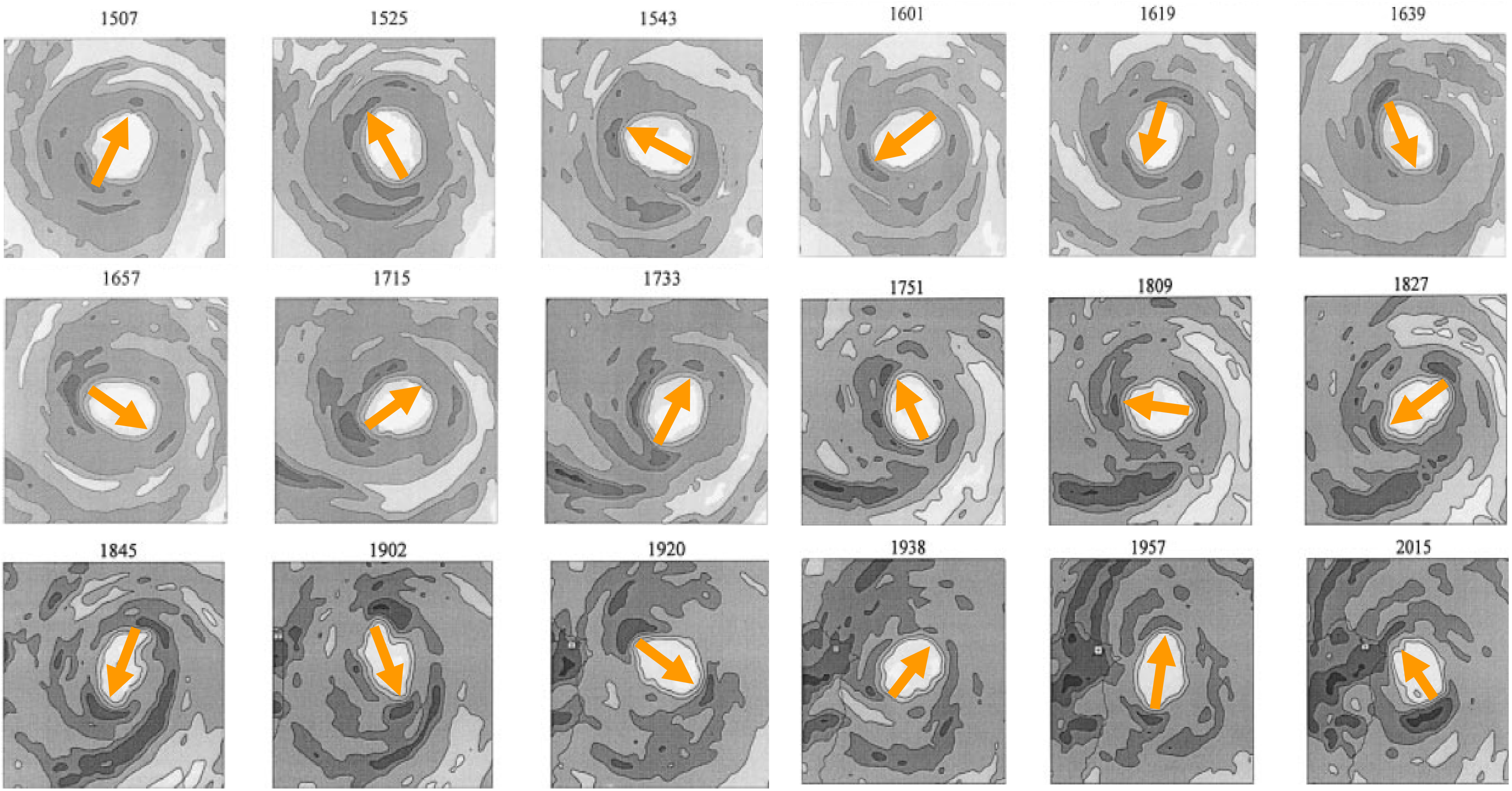

POLYGONAL EYEWALL (5)

Kossin & Eastin, 2001 [*J. Atmos. Sci.*, **58**, 1079-1090]

Aircraft flight level data show two distinct regimes of the kinematic and thermodynamic distribution within the eye and the eyewall :

- 1st regime : angular velocity is greatest within the eyewall and relatively depressed within the eye
- 2nd regime : radial profile of vorticity is nearly monotonic with maximum found at the eye center
- transition from 1st to 2nd regime can occur in less than 1 h, accompanied with dramatic changes in the thermodynamic structure

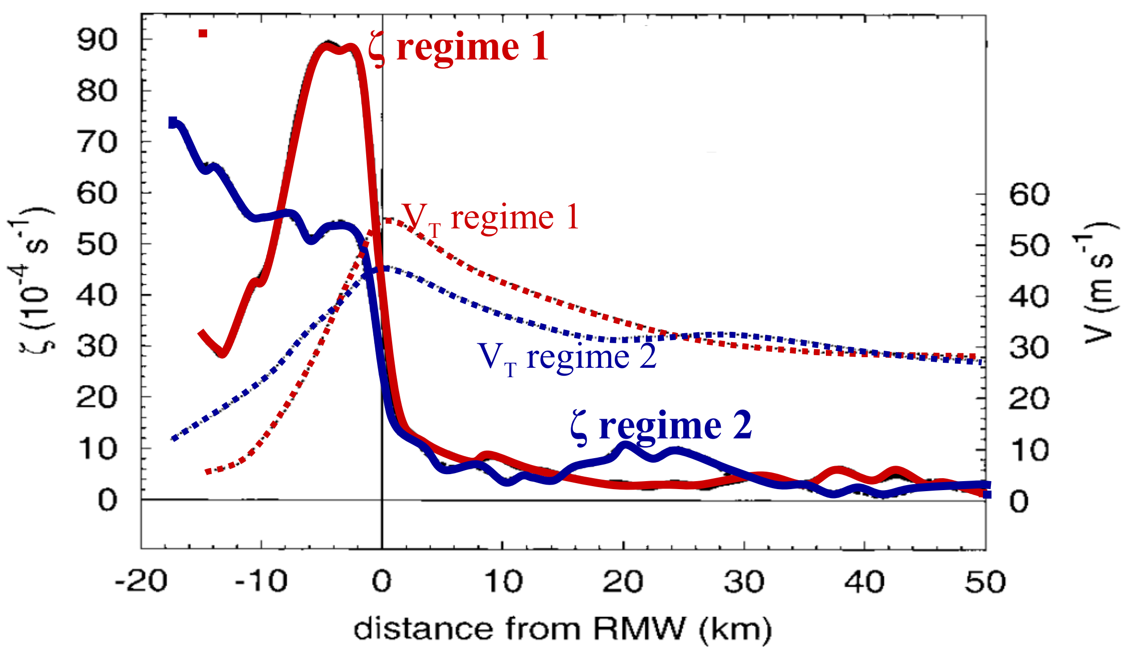

POLYGONAL EYEWALL (6)

- Regime 1 : the eye is warm and dry, θ_e is high in the eyewall and depressed in the eye

- Regime 2 : relative humidity is close to 100% everywhere, θ_e is maximum in the eye

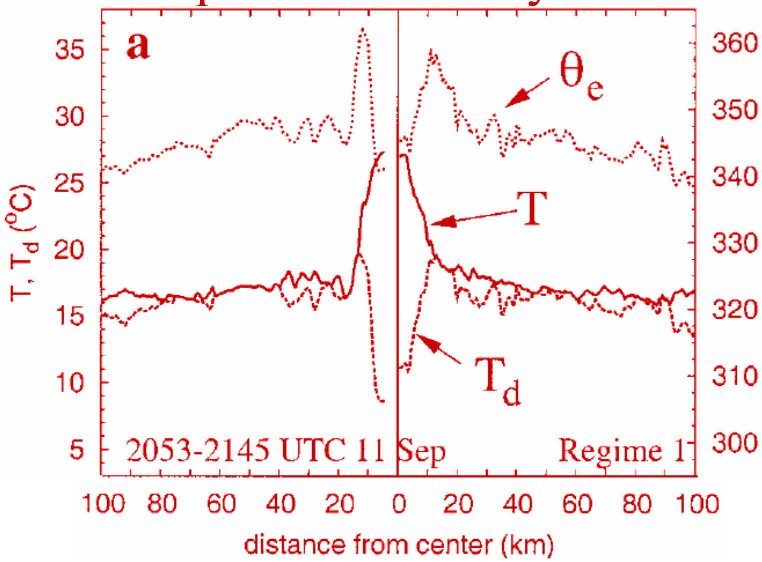

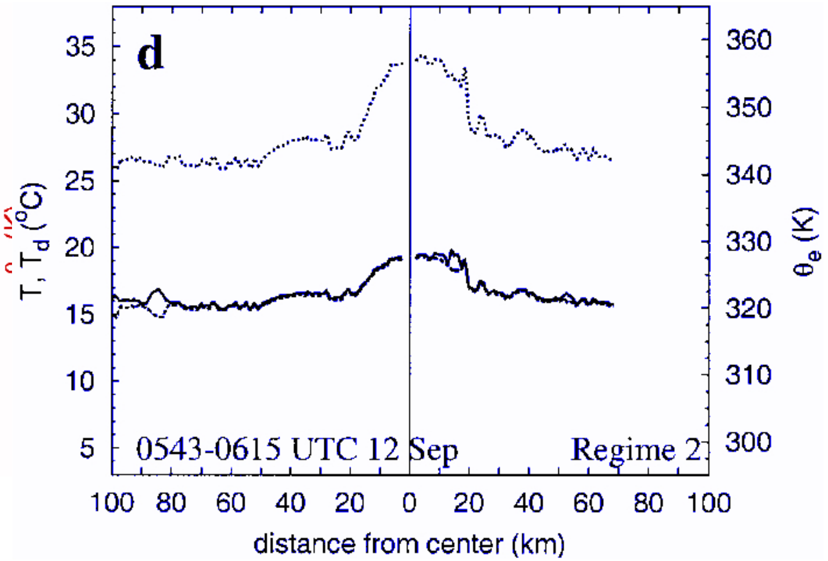

This evolution can be explained through horizontal vorticity mixing (idealized 2D barotropic framework)